ONLINE METHODS

Study subjects. Characteristics of each case-control group are shown in **Supplementary Table 1**.

RIKEN case samples. A total of 1,532 case subjects for the GWAS were recruited from the Miyatake Asthma Clinic, Miyagawa Clinic, Kyoto University Hospital, Tsukuba University Hospital and several other hospitals. All subjects with asthma were diagnosed by physicians according to the American Thoracic Society criteria as described[23].

BioBank Japan cases samples. The BioBank Japan project has been running since 2003 aiming at collection of basic information of patients for personalized medicine[24]. The subjects were recruited from several medical institutes in Japan, including the Fukujuji Hospital, Iizuka Hospital, Juntendo University, Hospital Iwate Medical University School of Medicine, National Hospital Organization Osaka National Hospital, Nihon University, Nippon Medical School, Shiga University of Medical Science, the Cancer Institute Hospital of the Japanese Foundation for Cancer Research, Tokushukai Hospital and Tokyo Metropolitan Geriatric Hospital. We selected case samples from the subjects who participated in the BioBank Japan. A total of 5,639 cases for replication study were recruited. All subjects with bronchial asthma were diagnosed by physicians and recruited in hospitals.

Controls. We used genome-wide screening data of the BioBank Japan project for control data. Individuals with bronchial asthma, allergic rhinitis, atopic dermatitis, lung fibrosis or chronic obstructive pulmonary disease were excluded from controls. Controls for the GWAS consisted of 2,403 cases from BioBank Japan and 901 healthy volunteers from members of the Rotary Club of Osaka-Midosuji District 2660 Rotary International in Japan[25]. Controls for the replication study consisted of 24,608 cases registered in BioBank Japan.

All individuals were Japanese and gave written informed consent to participate in the study. This research project was approved by the ethical committees at the Institute of Medical Science, the University of Tokyo and RIKEN Yokohama Institute.

Sample descriptions of Sepracor, LOCCS, LODO and Illumina. This cohort consisted of 499 non-Hispanic cases of European ancestry with mild to severe asthma from three adult asthma populations: (i) a medication trial conducted by Sepracor, Inc., US[26,27]; (ii) the Leukotriene Modifier or Corticosteroid Salmeterol (LOCCS) study[28]; and (iii) the Effectiveness of Low Dose Theophylline as an Add-on Treatment in Asthma (LODO) trial[28]. Cases were matched with 639 population controls obtained from Illumina's IconDB resource (see URLs) using the genetic matching (GEM) algorithm[29]. Genome-wide genotyping of cases was performed on the Illumina 610-Quad platform. Genome-wide genotyping of controls was performed on the Illumina HumanHap 550K v3 platform. Allelic model association statistics were calculated with PLINK[30]. The corresponding genetic inflation factor was 1.03, which shows minimal population stratification. Power calculations were performed using the Genetic Power Calculator[31] with the effect size as estimated in the primary combined GWAS, a disease prevalence of 0.05, $D' = 1$, marker allele frequency of cases, assuming use of unselected controls, and with default error rates ($\alpha = 0.05$ and power = 0.80).

Genotyping and quality control. For the GWAS, we genotyped 1,532 cases using the Illumina HumanHap610-Quad BeadChip and 3,304 controls using the Illumina HumanHap550 BeadChip. We excluded related samples by allele sharing analysis and performed principal component analysis for the genotype data of the samples along with European (CEU), African (YRI) and east Asian (Japanese (JPT) and Han Chinese (CHB)) individuals obtained from the Phase II HapMap database by using smartpca[32]. We excluded outliers who were away from the east Asian cluster (**Supplementary Fig. 1a**). We also excluded SNPs with minor allele frequencies of less than 0.01 in both cases and controls. SNPs having call rates ≥99% in both cases and controls were used for the association study. We conducted exact Hardy-Weinberg equilibrium analysis, and SNPs with P values less than the cut-off values of the Hardy-Weinberg equilibrium test ($P < 10^{-6}$ in controls) were excluded from the analysis.

In the replication study, we genotyped cases with asthma using the TaqMan assay (Applied Biosystems) or multiplex-PCR–based Invader assay (Third Wave Technologies). We calculated the concordance rates of the five SNPs in **Table 1** between genotypes determined by the Illumina HumanHap610-Quad BeadChip and those determined by the TaqMan assay (rs1837253, rs10508372 and rs1701704) or multiplex-PCR–based Invader assay (rs7686660 and rs404860). We genotyped a total of 1,532 cases in the GWAS, and the concordance rates were 1.000, 0.999, 1.000, 1.000 and 1.000, respectively. The concordance rate between the genotypes determined by the Illumina Human610-Quad BeadChip and Illumina HumanHap550v3 BeadChip among 182 duplicated samples was 0.99998 (ref. 25). Cluster plots of the GWAS for the five SNPs are shown in **Supplementary Figure 3**.

Statistical analysis. In the GWAS and replication study, the statistical significance of the association with each SNP was assessed using a 1-degree-of-freedom Cochran-Armitage trend test. ORs and CIs were calculated from a two-by-two allele frequency table. Combined analysis was conducted using the Mantel-Haenszel method and heterogeneity among studies was examined with the Breslow-Day test. We used Haploview 4.2 software to analyze the LD values between SNPs.

23. Harada, M. *et al.* A functional polymorphism in IL-18 is associated with severity of bronchial asthma. *Am. J. Respir. Crit. Care Med.* **180**, 1048–1055 (2009).
24. Nakamura, Y. The BioBank Japan Project. *Clin. Adv. Hematol. Oncol.* **5**, 696–697 (2007).
25. Takata, R. *et al.* Genome-wide association study identifies five new susceptibility loci for prostate cancer in the Japanese population. *Nat. Genet.* **42**, 751–754 (2010).
26. Silverman, E.S. *et al.* Transforming growth factor-beta1 promoter polymorphism C-509T is associated with asthma. *Am. J. Respir. Crit. Care Med.* **169**, 214–219 (2004).
27. Silverman, E.S. *et al.* Constitutive and cytokine-induced expression of the ETS transcription factor ESE-3 in the lung. *Am. J. Respir. Cell Mol. Biol.* **27**, 697–704 (2002).
28. Peters, S.P. *et al.* Randomized comparison of strategies for reducing treatment in mild persistent asthma. *N. Engl. J. Med.* **356**, 2027–2039 (2007).
29. Luca, D. *et al.* On the use of general control samples for genome-wide association studies: genetic matching highlights causal variants. *Am. J. Hum. Genet.* **82**, 453–463 (2008).
30. Purcell, S. *et al.* PLINK: a tool set for whole-genome association and population-based linkage analyses. *Am. J. Hum. Genet.* **81**, 559–575 (2007).
31. Purcell, S. *et al.* Genetic Power Calculator: design of linkage and association genetic mapping studies of complex traits. *Bioinformatics* **19**, 149–150 (2003).
32. Price, A.L. *et al.* Principal components analysis corrects for stratification in genome-wide association studies. *Nat. Genet.* **38**, 904–909 (2006).

nature genetics

Genome-wide association study identifies two susceptibility loci for exudative age-related macular degeneration in the Japanese population

Satoshi Arakawa[1,2], Atsushi Takahashi[3], Kyota Ashikawa[1], Naoya Hosono[1], Tomomi Aoi[1], Miho Yasuda[2], Yuji Oshima[2], Shigeo Yoshida[2], Hiroshi Enaida[2], Takashi Tsuchihashi[4], Keisuke Mori[4], Shigeru Honda[5], Akira Negi[5], Akira Arakawa[6], Kazuaki Kadonosono[6], Yutaka Kiyohara[7], Naoyuki Kamatani[3], Yusuke Nakamura[8], Tatsuro Ishibashi[2] & Michiaki Kubo[1]

Age-related macular degeneration (AMD), the leading cause of irreversible blindness in the world, is a complex disease caused by multiple environmental and genetic risk factors. To identify genetic factors that modify the risk of exudative AMD in the Japanese population, we conducted a genome-wide association study and a replication study using a total of 1,536 individuals with exudative AMD and 18,894 controls. In addition to *CFH* (rs800292, $P = 4.23 \times 10^{-15}$) and *ARMS2* (rs3750847, $P = 8.67 \times 10^{-29}$) loci, we identified two new susceptibility loci for exudative AMD: *TNFRSF10A-LOC389641* on chromosome 8p21 (rs13278062, combined $P = 1.03 \times 10^{-12}$, odds ratio = 0.73) and *REST-C4orf14-POLR2B-IGFBP7* on chromosome 4q12 (rs1713985, combined $P = 2.34 \times 10^{-8}$, odds ratio = 1.30). Fine mapping revealed that rs13278062, which is known to alter *TNFRSF10A* transcriptional activity, had the most significant association in 8p21 region. Our results provide new insights into the pathophysiology of exudative AMD.

AMD is a major cause of severe visual impairment among the elderly population in developed countries[1,2]. Late AMD is divided into exudative AMD and geographic atrophy, and the prevalences of these two types of AMD are different between the European and Asian populations[3,4]. Exudative AMD is a major type of late AMD in the Asian population and is characterized by abnormal vasculopathies arising from the choroidal vasculature, which may lead to recurrent serous exudation and hemorrhages[3]. In contrast, geographic atrophy is a common type of late AMD in the European population and is characterized by retinal pigment epithelium (RPE) atrophy and thinning of the retina without exudative or hemorrhagic changes. Although the inflammation of the RPE-choroid interface and the apoptosis of both photoreceptor and RPE cells have crucial roles in the development of AMD, the precise pathogenesis of AMD has not been fully elucidated[5,6].

Previous genome-wide association studies (GWAS) have identified many common variants in AMD risk[7–12]. Landmark GWAS identified *CFH* (complement factor H) and *ARMS2* (age-related maculopathy susceptibility 2) as the susceptibility genes for AMD[7,8]. Recent advances in genetic research have clarified that the variants of several complement pathway-associated genes have important roles in the pathogenesis of AMD[13–17]. Although previous GWAS have identified eight susceptibility loci for AMD, most of these findings included only the results from European populations[7–11]. Regardless of the differences in the prevalence of AMD type between European and Asian populations, there is scarce information for the susceptibility genes of AMD in the Asian population.

To investigate the genetic background of exudative AMD in the Japanese population, we conducted a GWAS to identify genes related to exudative AMD susceptibility using 827 cases and 3,323 controls. We genotyped these samples using the Illumina Human610-Quad BeadChip for cases and the Illumina HumanHap550v3 BeadChip for controls. Genotype concordance between these two BeadChips was 99.99% among 182 duplicate samples, indicating a low possibility of genotype error. After we applied stringent quality control criteria, we carried out an association analysis in 457,489 autosomal SNPs that were available on both BeadChips. Principal component analysis (PCA) showed no population substructure, and the quantile-quantile plot showed that the inflation factor was 1.057 (**Supplementary Fig. 1a,b**). To further examine the possibility of population substructure and its influence on our GWAS results, we performed PCA again using the HapMap JPT and CHB populations as the references. Almost all subjects fell into the known two main clusters of the Japanese population

[1]Laboratory for Genotyping Development, Center for Genomic Medicine, RIKEN Yokohama Institute, Yokohama, Japan. [2]Department of Ophthalmology, Graduate School of Medical Sciences, Kyushu University, Fukuoka, Japan. [3]Laboratory for Statistical Analysis, Center for Genomic Medicine, RIKEN Yokohama Institute, Yokohama, Japan. [4]Department of Ophthalmology, Saitama Medical University, Saitama, Japan. [5]Department of Surgery, Division of Ophthalmology, Kobe University Graduate School of Medicine, Kobe, Japan. [6]Department of Ophthalmology, Yokohama City University Medical Center, Yokohama, Japan. [7]Department of Environmental Medicine, Graduate School of Medical Sciences, Kyushu University, Fukuoka, Japan. [8]Laboratory of Molecular Medicine, Human Genome Center, Institute of Medical Science, University of Tokyo, Tokyo, Japan. Correspondence should be addressed to M.K. (mkubo@src.riken.jp).

Received 16 March; accepted 17 August; published online 11 September 2011; doi:10.1038/ng.938

Table 1 Summary of the GWAS and replication study

SNP	Allele	Minor allele	Chr.	Chr. location	Gene	Study	No. of samples		MAF		Age and sex adjusted			
							Case	Control	Case	Control	*P*	OR	95% CI	P_{het}
rs13278062	T/G	T	8	23,138,916	*TNFRSF10A-LOC389641*	GWAS	827	3,323	0.417	0.343	2.46×10^{-6}	0.71	0.62–0.82	
						Replication	701	15,565	0.417	0.346	8.19×10^{-8}	0.74	0.66–0.82	
						Combined					1.03×10^{-12}	0.73	0.67–0.80	0.68
rs1713985	T/G	G	4	57,481,207	*REST-C4orf14-POLR2B-IGFBP7*	GWAS	827	3,323	0.333	0.286	9.03×10^{-5}	1.34	1.16–1.56	
						Replication	708	15,569	0.329	0.282	5.71×10^{-5}	1.27	1.13–1.43	
						Combined					2.34×10^{-8}	1.30	1.19–1.42	0.56

The age- and sex-adjusted *P* values were calculated by logistic regression analysis under an additive model. The combined *P* values were calculated by the inverse variance method. The *P* values of heterogeneities (P_{het}) across the population were estimated formally using a Cochran's *Q* test. Chr., chromosome; No., number; MAF, minor allele frequency; OR, odds ratio; CI, confidence interval.

(**Supplementary Fig. 1c**). When we evaluated the quantile-quantile plot only using the samples in the main (Hondo) cluster, the inflation factor was 1.076 (**Supplementary Fig. 1d**). Therefore, we considered that genotype misclassification or population substructure might not be the cause of the difference in the inflation factor.

In our GWAS, two loci reached a genome-wide significant level of association ($P < 5 \times 10^{-8}$; **Supplementary Fig. 1g**). These two loci have already been reported in previous GWAS[7–12]: *ARMS2* (rs3750847, $P = 8.67 \times 10^{-29}$) and *CFH* (rs800292, $P = 4.23 \times 10^{-15}$). Results from these loci are shown in **Supplementary Figure 2**. We also checked the association of previously reported susceptibility loci for AMD (**Supplementary Table 1**). We found a significant association for three loci (*CFI*, *C2* and *CFB*), whereas we did not replicate susceptibility loci identified in recent GWAS of the European population (*TIMP3* and *LIPC*), probably because of the lower statistical power in our study. Notably, rs2230199, a marker SNP at the *C3* locus, was not polymorphic in the Japanese population. Although exudative AMD is a major type of AMD in Japanese compared to European individuals, these results indicate that the underlying disease mechanisms of AMD are largely similar for both populations, and the differences in genetic modifiers or environmental factors may represent the differences in the prevalence of a specific late-stage AMD type.

To identify additional susceptibility loci, we conducted a replication study using an independent set of 709 Japanese exudative AMD cases and 15,571 controls. Among 146 SNPs that showed $P < 1.0 \times 10^{-4}$ in GWAS, we selected 77 SNPs for the replication study after excluding 47 SNPs within the same locus ($r^2 > 0.8$) and 22 SNPs located at previously reported loci. We successfully genotyped all 77 SNPs using the multiplex PCR-based Invader assay and found significant association in two SNPs after Bonferroni correction (corrected $P < 6.49 \times 10^{-4}$; **Supplementary Table 2**). When we combined the results of the GWAS and a replication study by the inverse variance method, two SNPs reached a genome-wide significance level of association: rs13278062 on chromosome 8p21 (combined $P = 1.03 \times 10^{-12}$, odds ratio (OR) = 0.73, 95% confidence interval (CI) 0.67–0.80) and rs1713985 on chromosome 4q12 (combined $P = 2.34 \times 10^{-8}$, OR = 1.30, 95% CI 1.19–1.42; **Table 1**). The ORs between the GWAS and replication study were quite similar, and we did not observe any heterogeneity across the studies. A previous linkage study has also indicated an association on chromosome 8p21 (ref. 18).

Because exudative AMD is classified into typical AMD (t-AMD) and polypoidal choroidal vasculopathy (PCV), we found both SNPs showed a similar effect on susceptibility to each AMD subtype (**Supplementary Table 3**). Although we performed age-adjusted analysis, there is a possibility that aging or cohort effect might distort

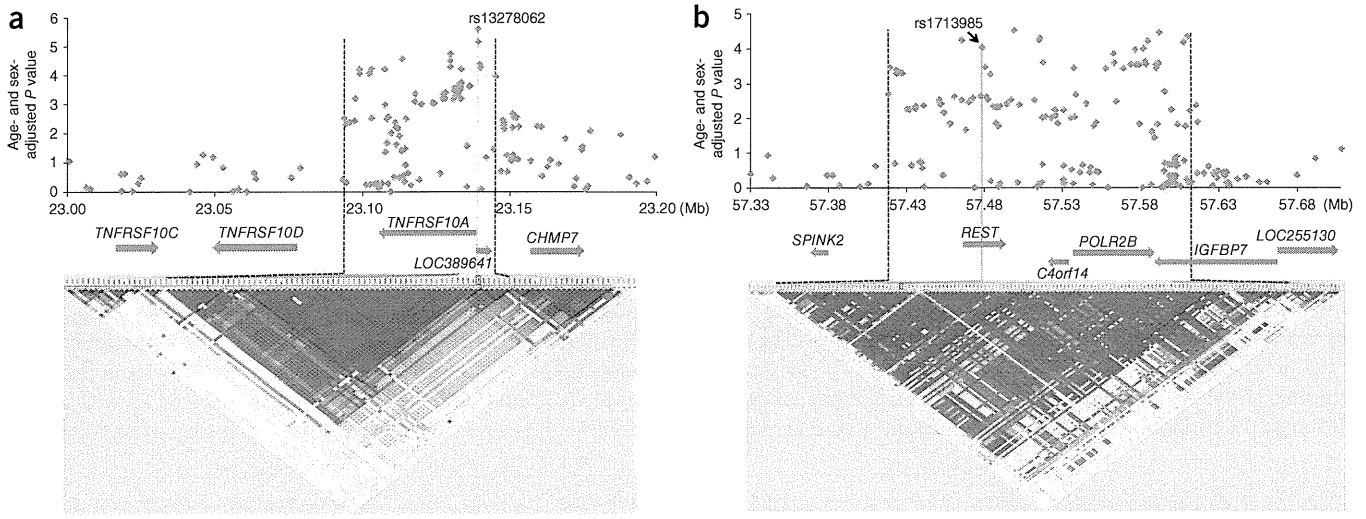

Figure 1 Case-control association plots, LD map and genomic structure of the *TNFRSF10A- LOC389641* region in chromosome 8p21 (**a**) and the *REST-C4orf14-POLR2B-IGFBP7* region in chromosome 4q12 (**b**). The candidate region is shown between the two black dashed lines. We performed fine mapping in the regions from 23.09–23.14 Mb in chromosome 8p21 and 57.42–57.61 Mb in chromosome 4q12. The blue diamonds represent $-\log_{10} P$ values obtained from GWAS and fine mapping. We drew the LD map based on *D'* values using the genotype data from the cases and controls in the GWAS samples. The blue lines indicate the position of the marker SNPs (rs13278062 (**a**) and rs1713985 (**b**)).

the findings of our study because the controls were younger than the cases, overall. However, we did not find marked differences in the minor allele frequencies (MAFs) of the two SNPs in each 10-year age group (**Supplementary Table 4**).

To narrow down the candidate regions and to identify susceptibility genes for exudative AMD, we carried out fine mapping using GWAS case-control samples. We first defined a linkage disequilibrium (LD) block and constructed a $-\log_{10} P$ plot of chromosome 8p21 using GWAS data. We found that the most highly associated SNP (rs13278062) represented an LD block that spanned from 23.078–23.152 Mb. Then, we selected and genotyped 18 SNPs around this LD block based on the data from the HapMap phase 2 Japanese population with a MAF ≥ 0.05. Next, we resequenced a 51-kb region from 23.094–23.145 Mb using 48 individuals with exudative AMD. After excluding repeat sequences, we identified 9 new SNPs in addition to the 88 known SNPs registered in the dbSNP database. After excluding 23 SNPs already genotyped, we genotyped 74 SNPs with MAF ≥ 0.05, and we successfully genotyped 73 of these. However, no SNPs showed stronger association than rs13278062 (**Fig. 1a** and **Supplementary Table 5a**). We also performed haplotype analysis using the four highly associated SNPs (rs2235126, rs7820465, rs13278062 and rs13281363), however, no haplotype showed stronger association than the single-marker association of rs13278062 (**Supplementary Fig. 3**).

rs13278062 is located in *LOC389641* and is also 397 bp upstream of *TNFRSF10A*, the tumor necrosis factor receptor superfamily 10a gene, which encodes one of the TRAIL receptors, TRAILR1. TRAILR1 is broadly expressed in human adult RPE[19] and rod photoreceptors in mice[20], whereas the expression of LOC389641 was low or absent according to the Gene Expression Omnibus (GEO) database. Binding of TRAIL to TRAILR1 is known to induce apoptosis through caspase 8 activation[21]. In addition, the TRAIL-TRAILR1 complex has a nonapoptotic pathway that induces the production of inflammatory cytokines and the promotion of inflammation through activation of nuclear factor B[22,23]. A previous study showed that the activator protein 1 will bind the sequence around rs13278062 and directly regulate TRAILR1 mRNA expression[24]. Moreover, the G allele of rs13278062 has been reported to enhance the transcriptional activity of TRAILR1 by 1.2- to 1.5-fold as compared to the T allele[25]. Although further functional studies are needed, these results speculate that *TNFRSF10A* is the susceptibility gene for exudative AMD and that rs13278062 may be the candidate of functional importance.

We observed the second most significant association at rs1713985 on chromosome 4q12. Based on the LD block and the $-\log_{10} P$ plot of chromosome 4q12 obtained by the GWAS data, we found that rs1713985 represents an LD block that spans from 57.421–57.611 Mb and includes four genes, *REST*, *C4orf14*, *POLR2B* and *IGFBP7* (**Fig. 1b**). Then, we selected and genotyped 120 SNPs around this LD block based on the data from the HapMap phase 2 Japanese population with MAF ≥ 0.05 (**Supplementary Table 5b**). However, this analysis could not narrow down the candidate region because of the long-range LD. According to the global expression profiles in GEO database, all four genes were expressed in human adult RPE[19] and rod photoreceptors in mice[20]. *REST* is a transcriptional repressor that may act as a master negative regulator of neurogeneisis. Overexpression of the *C4orf14* gene product has been reported to induce apoptosis by regulating mitochondrial nitric oxide and calcium[26]. The *IGFBP7* gene product, angiomodulin, is reported to bind chemokines and growth factors including vascular endothelial growth factor A, whose expression is high in RPE cells of AMD.

In conclusion, our data showed that *TNFRSF10A-LOC389641* on chromosome 8p21 and *REST-C4orf14-POLR2B-IGFBP7* on chromosome 4q12 are new susceptibility loci for exudative AMD in the Japanese population. Further functional studies are necessary to clarify the mechanisms of these loci on the susceptibility to exudative AMD.

URLs. GEO, http://www.ncbi.nlm.nih.gov/geo/; R statistical environment version 2.7.0, http://www.r-project.org/; PLINK 1.05, http://pngu.mgh.harvard.edu/~purcell/plink/; Genetic Power Calculator, http://pngu.mgh.harvard.edu/~purcell/gpc/; EIGENSTRAT, http://genepath.med.harvard.edu/~reich/Software.htm.

METHODS

Methods and any associated references are available in the online version of the paper at http://www.nature.com/naturegenetics/.

Accession codes. The expression microarray data on the human adult RPE and rod photoreceptors in mice have been deposited in the GEO database under accession numbers GSE18811 and GSE22317.

Note: Supplementary information is available on the Nature Genetics website.

ACKNOWLEDGMENTS

We thank all of the subjects who participated in this study. We are grateful to A. Yoshida, K. Kano, S. Kawahara, R. Arita, K. Ishikawa, E. Hasegawa, R. Asato, S. Notomi, T. Asakuma and A. Kuni of the Kyushu University, K. Horie-Inoue, S. Inoue and T. Awata of the Saitama Medical University, H. Bessho, N. Kondo and W. Matsumiya of the Kobe university and M. Inoue of the Yokohama City University Medical Center for collecting samples. We thank the staff of the Laboratory for Genotyping Development, Center for Genomic Medicine, RIKEN, the staffs of the BioBank Japan project and the members of the Rotary Club of Osaka-Midosuji District 2660 Rotary International in Japan. We want to express special thanks to F. Miya for the support of gene expression data. This work was conducted as a part of the BioBank Japan Project and supported by the Ministry of Education, Culture, Sports, Sciences and Technology of the Japanese government.

AUTHOR CONTRIBUTIONS

S.A., T.I., Y.N. and M.K. designed the study. S.A., N.H., K.A., T.A. and M.K. performed genotyping. S.A. and M.K. wrote the manuscript. A.T. performed statistical analysis at the genome-wide phase. Y.N. and M.K. managed DNA samples belonging to BioBank Japan. T.I. and Y.N. obtained funding for the study. M.Y., Y.O., S.Y. and H.E. collected GWAS samples. T.T., K.M., S.H., A.N., A.A. and K.K. collected case samples for the replication study. Y.K., N.K., Y.N. and M.K. supervised the study.

COMPETING FINANCIAL INTERESTS

The authors declare no competing financial interests.

Published online at http://www.nature.com/naturegenetics/.
Reprints and permissions information is available online at http://www.nature.com/reprints/index.html.

1. Wong, T.Y. *et al.* The natural history and prognosis of neovascular age-related macular degeneration. *Ophthalmology* **115**, 116–126 (2008).
2. Yuzawa, M. *et al.* Report on the nationwide epidemiological survey of exudative age-related macular degeneration in Japan. *Int. Ophthalmol.* **21**, 1–3 (1997).
3. Laude, A. *et al.* Polypoidal choroidal vasculopathy and neovascular age-related macular degeneration: same or different disease? *Prog. Retin. Eye Res.* **29**, 19–29 (2010).
4. Kawasaki, R. *et al.* The prevalence of age-related macular degeneration in Asians. A systematic review and meta-analysis. *Ophthalmology* **117**, 921–927 (2010).
5. Dunaief, J.L., Dentchev, T., Ying, G.S. & Milam, A.H. The role of apoptosis in age-related macular degeneration. *Arch. Ophthalmol.* **120**, 1435–1442 (2002).
6. Ding, X., Patel, M. & Chan, C.C. Molecular pathology of the age-related macular degeneration. *Prog. Retin. Eye Res.* **28**, 1–18 (2009).
7. Klein, R.J. *et al.* Complement factor H polymorphism in age-related macular degeneration. *Science* **308**, 385–389 (2005).
8. Dewan, A. *et al.* HTRA1 promoter polymorphism in wet age-related macular degeneration. *Science* **314**, 989–992 (2006).
9. Neale, B.M. *et al.* Genome-wide association study of advanced age-related macular degeneration identifies a role of the hepatic lipase gene (*LIPC*). *Proc. Natl. Acad. Sci. USA* **107**, 7395–7400 (2010).

10. Chen, W. *et al.* Genetic variants near *TIMP3* and high-density lipoprotein-associated loci influence susceptibility to age-related macular degeneration. *Proc. Natl. Acad. Sci. USA* **107**, 7401–7406 (2010).
11. Goto, A. *et al.* Genetic analysis of typical wet-type age-related macular degeneration and polypoidal choroidal vasculopathy in Japanese population. *J. Ocul. Biol. Dis. Infor.* **2**, 164–175 (2009).
12. Kopplin, L.J. *et al.* Genome-wide association identifies *SKIV2L* and *MYRIP* as protective factors for age-related macular degeneration. *Genes Immun.* **11**, 609–621 (2010).
13. Fritsche, L.G. *et al.* An imbalance of human complement regulatory proteins CFHR1, CFHR3 and factor H influences risk for age-related macular degeneration (AMD). *Hum. Mol. Genet.* **19**, 4694–4704 (2010).
14. Gold, B. *et al.* Variation in factor B (*BF*) and complement component 2 (*C2*) genes is associated with age-related macular degeneration. *Nat. Genet.* **38**, 458–462 (2006).
15. Montes, T., Tortajada, A., Morgan, B.P., Rodriguez de Cordoba, S. & Harris, C.L. Functional basis of protection against age-related macular degeneration conferred by a common polymorphism in complement factor B. *Proc. Natl. Acad. Sci. USA* **106**, 4366–4371 (2009).
16. Spencer, K.L. *et al.* C3 R102G polymorphism increases risk of age-related macular degeneration. *Hum. Mol. Genet.* **17**, 1821–1824 (2008).
17. Fagerness, J.A. *et al.* Variation near complement factor I is associated with risk of advanced AMD. *Eur. J. Hum. Genet.* **17**, 100–104 (2009).
18. Seddon, J.M., Santangelo, S.L., Book, K., Chong, S. & Cote, J. A genome-wide scan age-related macular degeneration provides evidence for linkage to several chromosomal regions. *Am. J. Hum. Genet.* **73**, 780–790 (2003).
19. Strunnikova, N.V. *et al.* Transcriptome analysis and molecular signature of human retinal pigment epithelium. *Hum. Mol. Genet.* **19**, 2468–2486 (2010).
20. Parapuram, S.K. *et al.* Distinct signature of altered homeostasis in aging rod photoreceptors: implications for retinal diseases. *PLoS ONE* **5**, e13885 (2010).
21. Johnstone, R.W., Frew, A.J. & Smyth, M.J. The TRAIL apoptotic pathway in cancer onset, progression and therapy. *Nat. Rev. Cancer* **8**, 782–798 (2008).
22. Chaudhary, P.M. *et al.* Death receptor 5, a new member of the TNFR family, and DR4 induce FADD-dependent apoptosis and activate the NF-B pathway. *Immunity* **7**, 821–830 (1997).
23. Li, J.H., Kirkiles-Smith, N.C., McNiff, J.M. & Pober, J.S. TRAIL induces apoptosis and inflammatory gene expression in human endothelial cells. *J. Immunol.* **171**, 1526–1533 (2003).
24. Guan, B., Yue, P., Lotan, R. & Sun, S.Y. Evidence that the human death receptor 4 is regulated by activator protein 1. *Oncogene* **21**, 3121–3129 (2002).
25. Wang, M. *et al.* Genetic variants in the death receptor 4 gene contribute to susceptibility to bladder cancer. *Mutat. Res.* **661**, 85–92 (2009).
26. Parihar, A., Parihar, M.S., Chen, Z. & Ghafourifar, P. mAtNOS1 induces apoptosis of human mammary adenocarcinoma cells. *Life Sci.* **82**, 1077–1082 (2008).

ONLINE METHODS

Samples. Characteristics of the study subjects are shown in **Supplementary Table 6**. For the GWAS, 827 individuals with exudative AMD were collected at Kyushu University. The diagnosis of exudative AMD was based on comprehensive ophthalmic examination, including fluorescein angiography and indocyanine green angiography findings and optical coherence tomography after pupil dilation. We classified exudative AMD into four subtypes under established criteria[27–30]: typical neovascular AMD (t-AMD), polypoidal choroidal vasculopathy (PCV), retinal angiomatous proliferation (RAP) and unclassified. In 827 individuals from the GWAS, we found 298 cases with t-AMD, 480 with PCV, 14 with RAP and 23 unclassified cases. Among these, we found 12 cases that had different subtypes in each eye. Cases with other macular diseases such as high myopia, angioid streaks and central serous chorioretinopathy were excluded. For the control subjects, we used genome-wide screening data of BioBank Japan samples, which consists of 2,421 individuals with thirteen diseases and 902 healthy volunteers recruited from Osaka-Midousuji Rotary Club, Osaka, Japan[31]. Disease status in the control group did not affect the MAFs of the SNPs (**Supplementary Table 7**).

For the replication study, 709 individuals with exudative AMD were recruited at Saitama Medical University (n = 396), Kobe University (n = 212) and Yokohama City University Medical Center (n = 101) under the same criteria as the GWAS cases. The numbers of exudative AMD subtypes were n = 325 for t-AMD, n = 358 for PCV, n = 3 for RAP and n = 23 for an unclassified subtype. We also used genome-wide screening data of BioBank Japan data, which consists of 15,571 individuals with one of ten diseases (colorectal cancer, breast cancer, prostate cancer, lung cancer, stomach cancer, diabetes, arteriosclerosis obliterans, atrial fibrillation, cerebral infarction and myocardial infarction) as controls.

All control individuals had not had a recent eye examination, and therefore it is unknown what ocular conditions, including AMD, were present in these individuals. Moreover, controls were significantly younger than cases, which indicates that some of the controls will go onto develop AMD as they age, although the incidence of late AMD is low in the Japanese population[32]. Because these limitations will underestimate the impact of SNPs on the development of late AMD, the true associations may be stronger than those shown in this study.

All participants provided written informed consent to participate in this study. This study was approved by the ethical committees of Kyushu University, Saitama Medical University, Kobe University, Yokohama City University Medical Center, Institute of Medical Science, the University of Tokyo and the RIKEN Yokohama Institute.

SNP genotyping. For the GWAS, we genotyped 832 individuals with exudative AMD using an Illumina Human610-Quad BeadChip, and we genotyped 3,323 controls using the Illumina HumanHap550v3 BeadChip. Although the call rate was ≥0.98 for all cases and controls, five cases were excluded because of paired closely related samples. Among the common SNPs in both BeadChips, 457,489 SNPs in the autosomal chromosomes passed the quality control filters (call rate ≥0.99 in both cases and controls and Hardy-Weinberg equilibrium $P \geq 1.0 \times 10^{-6}$ in controls) and were further analyzed. For the replication study, we selected 146 SNPs that showed an age- and sex-adjusted $P < 1.0 \times 10^{-4}$ in the GWAS. Among these SNPs, 22 were located at previously reported loci[7–12] and were excluded from further study. We calculated the LD coefficient (r^2) between the remaining SNPs and selected the 77 SNPs with the lowest P value within each region of $r^2 \geq 0.8$. In the replication study, we genotyped an additional panel of 709 individuals with exudative AMD using the multiplex PCR-based Invader assay[33] (Third Wave Technologies). We regarded genotyping as having been successful when the number of undetermined samples was less than 10 in a 384-well plate.

Fine mapping and resequencing. For the fine mapping, we used all case and control samples in the GWAS. Tagging SNPs were selected from those with MAF ≥ 5% in the region of interest based on the HapMap phase 2 JPT population. Resequencing of the candidate regions was performed in 48 exudative AMD cases by using an ABI3730 Genetic Analyzer.

Statistical analysis. In all stages, the associations of each SNP were assessed by age- and sex-adjusted logistic regression analysis under an additive model. The combined analysis of the GWAS and the replication study was conducted using the inverse variance method. Heterogeneities across the population were estimated formally by using a Cochran's Q test. To characterize the population structure, we computed genome-wide average identity by state and performed PCA using the EIGENSTRAT program (see URLs). GWAS and replication data were calculated using R statistical environment version 2.7.0 or PLINK 1.05 software[34]. Haploview software was used to analyze LD values[35].

27. Yannuzzi, L.A. *et al.* Polypoidal choroidal vasculopathy and neovascularized age-related macular degeneration. *Arch. Ophthalmol.* **117**, 1503–1510 (1999).
28. Yannuzzi, L.A. *et al.* Retinal angiomatous proliferation in age-related macular degeneration. *Retina* **21**, 416–434 (2001).
29. Sato, T., Kishi, S., Watanabe, G., Matsumoto, H. & Mukai, R. Tomographic features of branching vascular networks in polypoidal choroidal vasculopathy. *Retina* **27**, 589–594 (2007).
30. Matsumoto, H., Sato, T. & Kishi, S. Tomographic features of intraretinal neovascularization in retinal angiomatous proliferation. *Retina* **30**, 425–430 (2010).
31. Nakamura, Y. The BioBank Japan Project. *Clin. Adv. Hematol. Oncol.* **5**, 696–697 (2007).
32. Yasuda, M. *et al.* Nine-year incidence and risk factors for age-related macular degeneration in a defined Japanese population: the Hisayama Study. *Ophthalmology* **116**, 2135–2140 (2009).
33. Ohnishi, Y. *et al.* A high-throughput SNP typing system for genome-wide association studies. *J. Hum. Genet.* **46**, 471–477 (2001).
34. Purcell, S. *et al.* PLINK: a tool set for whole-genome association and population-based linkage analysis. *Am. J. Hum. Genet.* **81**, 559–575 (2007).
35. Barrett, J.C., Fry, B., Maller, J. & Daly, M.J. Haploview: analysis and visualization of LD and haplotype maps. *Bioinfomatics* **21**, 263–265 (2005).

Available online at www.sciencedirect.com
ScienceDirect
Metabolism Clinical and Experimental 60 (2011) 394–403
Metabolism
Clinical and Experimental
www.metabolismjournal.com

Short-term adenosine monophosphate–activated protein kinase activator 5-aminoimidazole-4-carboxamide-1-β-D-ribofuranoside treatment increases the sirtuin 1 protein expression in skeletal muscle

Masataka Suwa[a,*], Hiroshi Nakano[b], Zsolt Radak[c], Shuzo Kumagai[d]

[a]*Faculty of Life Design, Tohoku Institute of Technology, 6 Futatsusawa, Taihaku-ku, Sendai, Miyagi, 982-8588, Japan*
[b]*Department of Human Development, Nakamura Gakuen University, Jonan-ku, Fukuoka 814-0198, Japan*
[c]*Institute of Sport Science, Faculty of Physical Education and Sport Science, Semmelweis University, Budapest, Hungary*
[d]*Institute of Health Science, Kyushu University, Kasuga, Fukuoka 816-8580, Japan*

Received 3 April 2009; accepted 2 March 2010

Abstract

Adenosine monophosphate–activated protein kinase (AMPK) has been proposed to stimulate mitochondrial biogenesis and fat and glucose metabolism in skeletal muscle. Nicotinamide adenine dinucleotide–dependent histone deacetylase sirtuin 1 (SIRT1) is also thought to play a pivotal role for such metabolic adaptations. The purpose of the present study was to examine the effect of AMPK activation with the administration of AMPK activator 5-aminoimidazole-4-carboxamide-1-β-D-ribofuranoside (AICAR) to rats on skeletal muscle SIRT1 protein expression as well as peroxisome proliferator activated receptor γ coactivator–1α (PGC-1α) and glucose transporter 4 (GLUT4) protein expression and hexokinase activity. The AICAR promoted the phosphorylation of AMPK α-subunit (Thr^{172}) and acetyl–coenzyme A carboxylase (Ser^{79}) without any change of total AMPK α-subunit or acetyl–coenzyme A carboxylase protein levels in both the slow-twitch soleus and fast-twitch extensor digitorum longus (EDL) muscles. The SIRT1 protein expression increased at 24 hours after administration of AICAR in the EDL muscle but not in the soleus muscle. The PGC-1α protein expression increased in both the soleus and EDL muscles and GLUT4 did in the EDL muscle at 24 hours after an administration of AICAR. The hexokinase activity increased at 18 and 24 hours in the soleus and at 12, 18, and 24 hours in the EDL after an AICAR treatment. These results suggest that short-term AICAR treatment to rats promotes skeletal muscle AMPK phosphorylation and then coincidently increases the SIRT1 protein expression. In addition, such treatment also enhances the PGC-1α and GLUT4 protein contents and hexokinase activity in skeletal muscle.

1. Introduction

Silence information regulator 2 (Sir2) proteins are the nicotinamide adenine dinucleotide–dependent acetylases that regulate longevity in *Caenorhabditis elegans* [1] and *Saccharomyces cerevisiae* [2] in response to caloric restriction. In mammals, the Sir2 ortholog, sirtuin 1 (SIRT1)/Sir2α plays an important role in various biological processes via functionally interacting and deacetylating several proteins [3]. SIRT1 controls both energy homeostasis and metabolic adaptations [4]. The activation of SIRT1 with its activator resveratrol improved the glucose tolerance and survival in mice fed high-fat diet [5,6]. SIRT1 can promote mitochondrial biogenesis and fatty acid oxidation in skeletal muscle cells via deacetylation and functionally activating the peroxisome proliferator activated receptor γ coactivator–1α (PGC-1α) [7-9]. This metabolic role of SIRT1 is associated with 5′-adenosine monophosphate–activated protein kinase (AMPK), which is also a key regulator of energy metabolism [4].

5′-Adenosine monophosphate–activated protein kinase is a heterotrimer consisting of 3 subunits: α, β, and γ [10]. Two isoforms exist for both the α-subunit (α1 and α2) and β-subunit (β1 and β2) and 3 for the γ-subunit (γ1, γ2, and γ3). The α-subunit contains the catalytic domain. The β-subunit mediates the assembly of the heterotrimeric AMPK complex [11] and glycogen binding [12]. The γ-subunit binds the AMP and following phosphorylation of threonine

* Corresponding author. Tel.: +81 22 304 5599; fax: +81 22 304 5591.
E-mail address: suwa-m@tohtech.ac.jp (M. Suwa).

0026-0495/$ – see front matter.
doi:10.1016/j.metabol.2010.03.003

172 in the α-subunit and kinase activation [13]. The AMPK functions as an energy sensor and is activated when the cellular AMP to adenosine triphosphate ratio is increased [10]. The phosphorylation of threonine 172 in α-subunit strongly correlates with the AMPK activity [14]. The AMPK phosphorylation is mainly regulated by an upstream kinase LKB1 in skeletal muscle [15]. Skeletal muscle AMPK is activated by exercise [16], adipocytokines including leptin [17] and adiponectin [18], and antidiabetic drug metformin [19,20]. The activation of AMPK by its activator 5-aminoimidazole-4-carboxamide-1-β-D-ribofuranoside (AICAR) stimulates both glucose uptake and fatty acid oxidation in skeletal muscle cells [21] and increases insulin-stimulated glucose uptake, insulin signaling such as phosphatidylinositol 3-kinase and protein kinase B activities, glucose transporter 4 (GLUT4) protein expression, hexokinase activity, and mitochondrial oxidative enzyme activities in skeletal muscle [22-24]. The activation of AMPK by AICAR also increases the PGC-1α expression in skeletal muscle [25], which controls mitochondrial biogenesis and glucose metabolism [25,26]. The AMPK is indirectly phosphorylated by SIRT1 through LKB1 deacetylation [27]. In addition, AMPK promotes SIRT1 activation by enhancing the transcription and activity of nicotinamide phosphoribosyltransferase [28].

The skeletal muscle SIRT1 protein expression [29] and activity [30] have been observed to increase with endurance exercise in rat skeletal muscle. Endurance exercise has a great impact on the skeletal muscle metabolic characteristics, including mitochondrial biogenesis and GLUT4 expression [31], while also activating AMPK [16]. The activation of AMPK with AICAR also induces such metabolic adaptations in skeletal muscle [23,24], thus suggesting that the activation of AMPK mediates the effect of endurance exercise training on metabolic characteristics. It is hypothesized that AMPK regulates SIRT1 expression. The purpose of the present study was to investigate whether the activation of AMPK with short-term AICAR treatment to rats induced the expression of SIRT1 protein as well as the expression of PGC-1α and GLUT4 protein and also the hexokinase activity in slow- and fast-twitch skeletal muscles.

2. Materials and methods

2.1. Animals

Male Wistar rats that were 4 weeks of age and with a body weight of 70 to 90 g (Kyudo, Tosu, Saga, Japan) were used for the current study. All rats were handled daily for at least 5 days before beginning their experiment regimen. All rats were housed in a temperature- (22°C ± 2°C) and humidity- (60% ± 5%) controlled room with a 12-hour light (7:00 AM-7:00 PM) and 12-hour dark (7:00 PM-7:00 AM) cycle. Food and water were provided ad libitum. All experimental procedures were strictly conducted in accordance with the Nakamura Gakuen University Guidelines for the Care and Use of Laboratory Animals and were approved by the University Animal Experiment Committee.

2.2. AMPK and acetyl–coenzyme A carboxylase phosphorylation study

The rats were randomly assigned to pre (n = 12) and AICAR treatment (n = 36) groups. The rats of AICAR treatment group were then given a subcutaneous ingestion of AICAR (Toronto Research Chemicals, North York, Ontario, Canada; 1 mg/g body weight). The rats were anesthetized with pentobarbital sodium (60 mg/kg body weight IP), and the slow-twitch soleus and fast-twitch extensor digitorum longus (EDL) muscles were rapidly dissected out at 1 (n = 12), 2 (n = 12), and 4 (n = 12) hours after the AICAR treatment. The rats of the pre group were also anesthetized, and the soleus and EDL muscles were dissected out. The muscles were frozen in liquid nitrogen and stored at −80°C until determinations of phosphorylated and total AMPKα and acetyl–coenzyme A carboxylase (ACC) protein expression were performed.

A lysis buffer was used to inhibit phosphatases and determine the phosphorylated AMPK and ACC protein levels as well as total AMPKα and ACC (50 mmol/L HEPES, 0.1% Triton X-100, 4 mmol/L EGTA, 10 mmol/L EDTA, 15 mmol/L $Na_4P_2O_7$, 100 mmol/L β-glycerophosphate, 25 mmol/L NaF, 5 mmol/L Na_3VO_4, and 1 tablet per 50 mL Complete Protease Inhibitor Cocktail Tablets [Roche Diagnostics, Tokyo, Japan], pH 7.4). The muscle specimens were homogenized in ice-cold lysis buffer (1:10 wt/vol) with a Polytron-type homogenizer operating at maximum speed for 30 seconds. The homogenate was centrifuged at 15 000*g* (4°C) for 25 minutes. The protein concentration of the supernatant was then determined by use of a protein determination kit (Bio-Rad, Richmond, CA). The muscle protein homogenate was solubilized in sample loading buffer (50 mmol/L Tris-HCl, pH 6.8, 2% sodium dodecyl sulfate (SDS), 10% glycerol, 5% β-mercaptoethanol, and 0.005% bromophenol blue).

2.3. SIRT1, PGC-1α, and GLUT4 proteins and hexokinase activity study

The rats were randomly assigned to pre (n = 12), AICAR treatment (n = 48), and saline treatment (n = 12) groups. The rats of AICAR treatment group were then given a subcutaneous ingestion of AICAR (1 mg/g body weight). The rats were anesthetized with pentobarbital sodium (60 mg/kg body weight IP); and then the soleus and EDL muscles were rapidly dissected out at 6 (n = 12), 12 (n = 12), 18 (n = 12), and 24 (n = 12) hours after the AICAR treatment. The rats of pre group were also anesthetized, and the muscles were dissected out. In the rats of saline treatment group, a comparable volume of saline was administered subcutaneously. The rats were anesthetized, and the muscles were dissected out at 24 hours after the saline injection. The

muscles were frozen in liquid nitrogen and stored at −80°C until analyses were performed.

The frozen samples were homogenized with homogenizer in ice-cold homogenizing buffer (1:10 wt/vol) (25 mmol/L HEPES, 250 mmol/L sucrose, 2 mmol/L EDTA, 0.1% Triton X-100, and 1 tablet per 50 mL Complete Protease Inhibitor Cocktail Tablets [Roche Diagnostics], pH 7.4). The homogenate was centrifuged at 15000*g* (4°C) for 25 minutes. The protein concentration of the supernatant was determined by the use of a protein determination kit (Bio-Rad). The muscle homogenate was used for Western blotting to determine the SIRT1, PGC-1α, and GLUT4 protein contents and hexokinase activity. For Western blotting, the muscle protein homogenate was solubilized in sample loading buffer as described above.

2.4. Gel electrophoresis and Western blotting

The proteins (20 μg) of these homogenates were separated by SDS polyacrylamide gel electrophoresis using 5% (phospho- and total ACC), 7.5% (SIRT1 and PGC-1α), and 10% (GLUT4 and phospho- and total AMPKα) resolving gels. The proteins separated by SDS polyacrylamide gel electrophoresis were then electrophoretically transferred onto the polyvinylidene difluoride membrane. The membrane was incubated with a blocking buffer of casein solution (SP-5020; Vector Laboratories, Burlingame, CA) for 1 hour at room temperature. The membrane was reacted with affinity-purified rabbit polyclonal antibody to phospho-AMPKα (Thr^{172}; 1:500 dilution, #2532, Cell Signaling, Beverly, MA), total AMPKα (1:1000 dilution, #2531S, Cell Signaling), phospho-ACC (Ser^{79}; 1:500 dilution, #3661, Cell Signaling), total ACC (1:500 dilution, #3662, Cell Signaling), Sir2 (1:1000 dilution, #07-131, Upstate Biotechnology, Lake Placid, NY), PGC-1α (1:500 dilution, AB3242, Chemicon International, Temecula, CA), or GLUT4 (1:8000 dilution, AB1346, Chemicon International) overnight at 4°C and then was incubated with biotinylated anti-rabbit/mouse immunoglobulin G (1:1000 dilution, BA-1400, Vector

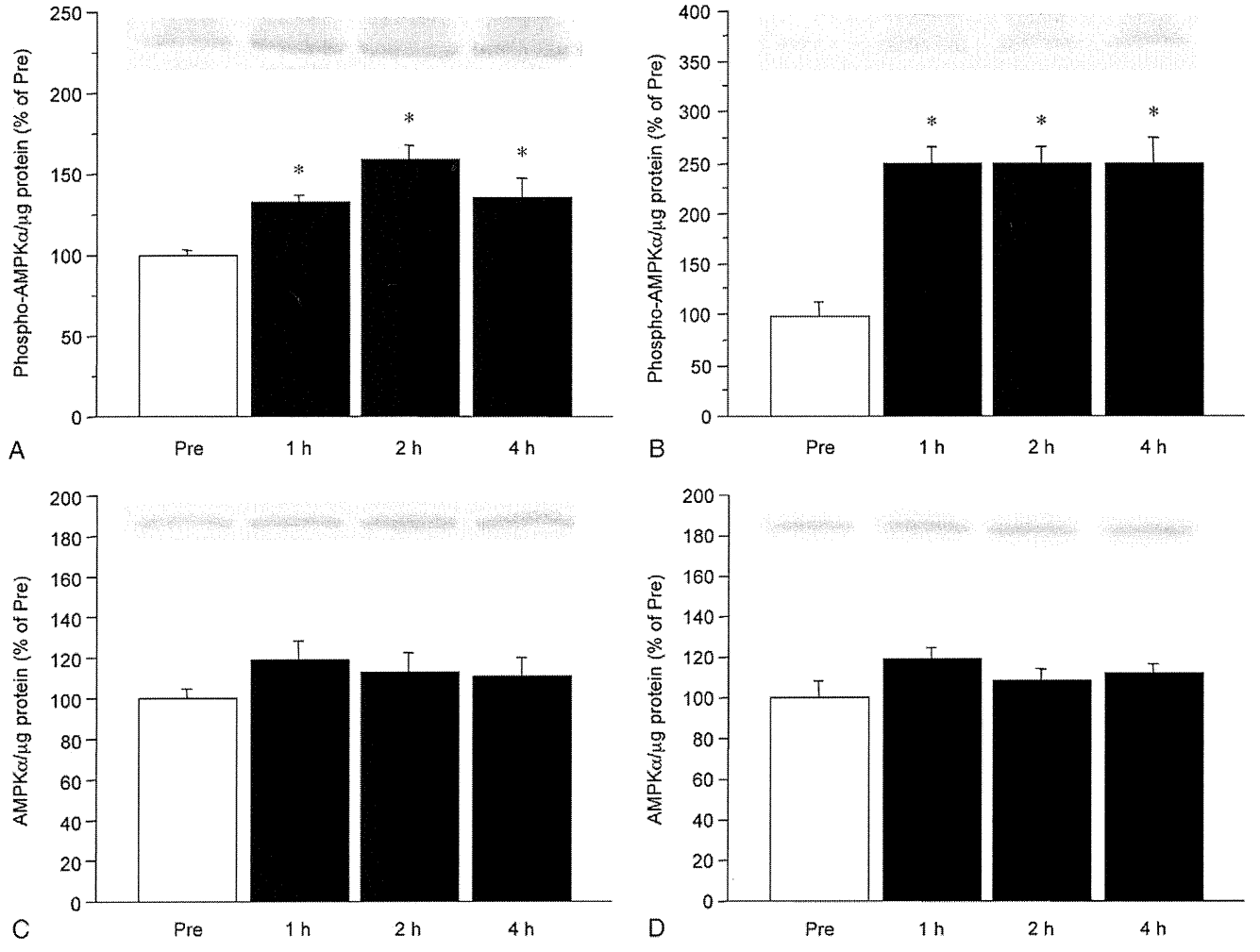

Fig. 1. Phospho- and total AMPKα protein expression in the soleus and EDL muscles before and 1, 2, and 4 hours after AICAR treatment. A and B, Phospho-AMPKα in soleus and EDL muscles, respectively. C and D, Total AMPKα in soleus and EDL muscles, respectively. Values are the means ± SE; n = 12 muscles per group. *$P < .05$ vs pre.

Laboratories) for 30 minutes. The band on the membrane was visualized by avidin and biotinylated horseradish peroxidase macromolecular complex technique (PK-6100, Vector Laboratories). The band densities were determined using the Image 1.62 software package (National Institute of Health, Bethesda, MD).

2.5. Hexokinase activity

The hexokinase activity was measured spectrophotometrically. The enzymatic assay was carried out at 30°C using saturating concentrations of substrates and cofactors as determined in preliminary analyses. The hexokinase activity was measured at 340 nm by following the production of reduced form of beta-nicotinamide adenine dinucleotide phosphate (NADPH) for 3 minutes. The extinction coefficient for NADPH, which is a reference of the hexokinase activity, was 6.22. For the hexokinase assay, 100 mmol/L Tris-HCl, 0.4 mmol/L beta-nicotinamide adenine dinucleotide phosphate (NADP), 5 mmol/L $MgCl_2$, 700 U/mL glucose-6-phosphate dehydrogenase, 1 mmol/L glucose (omitted for the measurement of nonspecific activity), and 5 mmol/L adenosine triphosphate (omitted for the measurement of nonspecific activity), pH 7.0, were used.

2.6. Statistical analysis

All data are expressed as the means ± SE. To estimate the time course of the protein expressions and hexokinase activity with AICAR treatment, we used the 1-way analysis of variance. Dunnett post hoc test was conducted if the analysis of variance indicated a significant difference. The unpaired t test was used to compare the saline and AICAR groups. A value of $P < .05$ was considered to be significant.

3. Results

3.1. AMPK and ACC protein phosphorylation

Fig. 1 shows the change in the phosphorylated and total AMPKα protein expression after an AICAR treatment. In the

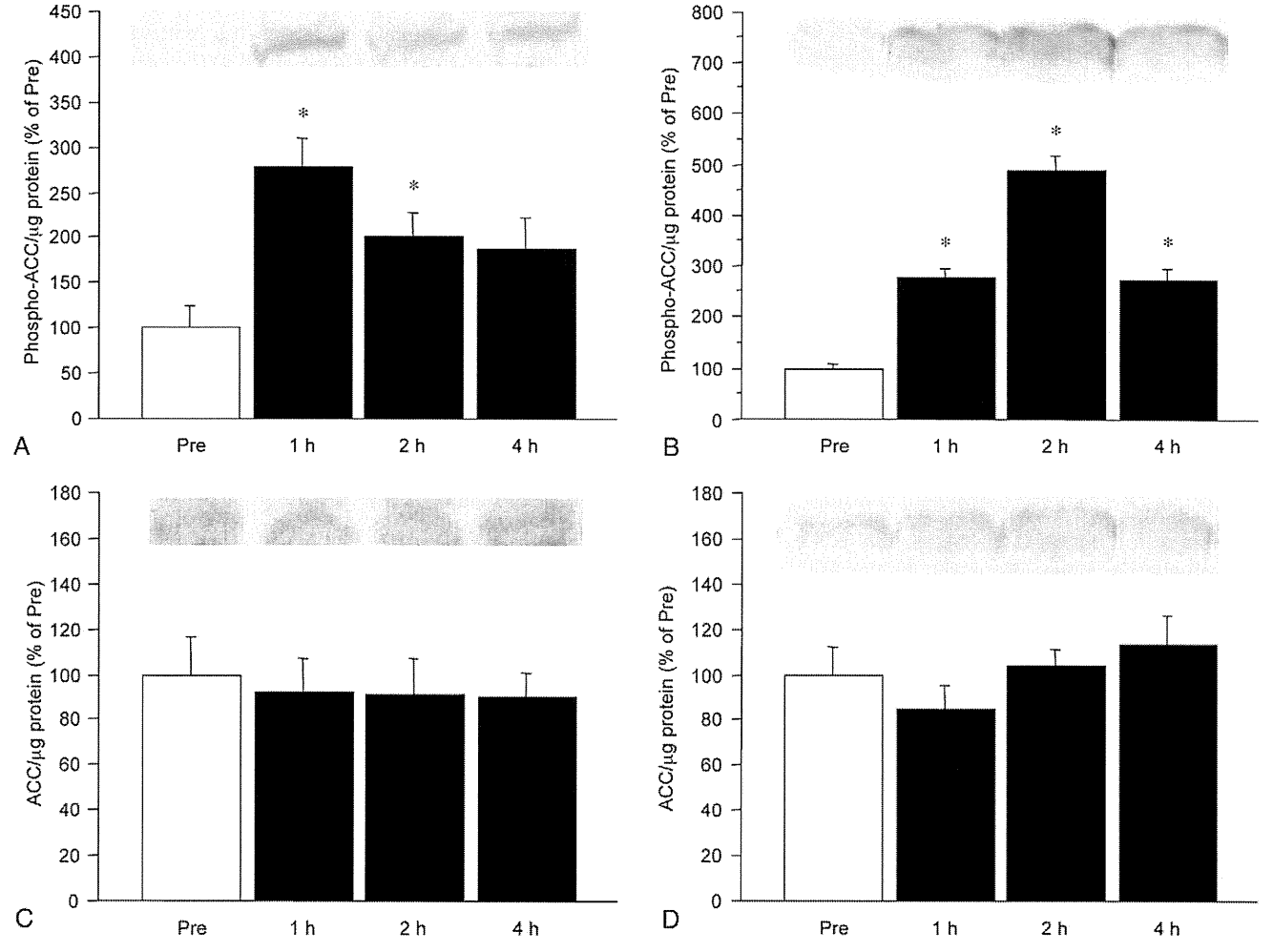

Fig. 2. Phospho- and total ACC protein expression in soleus and EDL muscles before and 1, 2, and 4 hours after AICAR treatment. A and B, Phospho-ACC in soleus and EDL muscles, respectively. C and D, Total ACC in soleus and EDL muscles, respectively. Values are the means ± SE; n = 12 muscles per group. *$P <$ .05 vs pre.

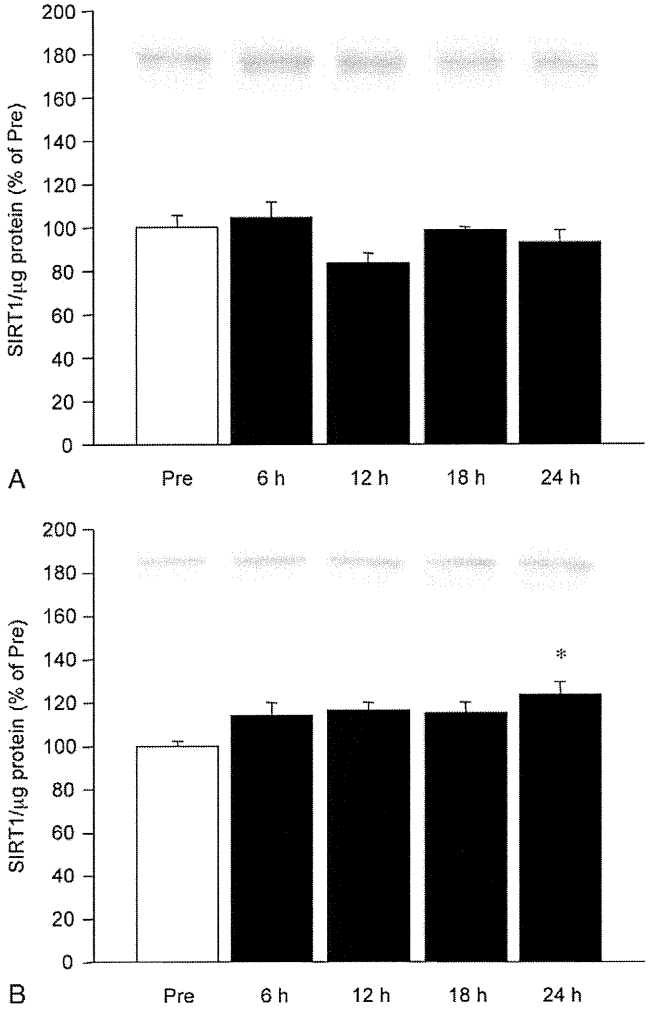

Fig. 3. SIRT1 protein expression in the soleus (A) and EDL (B) muscles before and 6, 12, 18, and 24 hours after AICAR treatment. Values are the means ± SE; n = 12 muscles per group. *$P < .05$ vs pre.

soleus muscle, the phosphorylated AMPKα protein increased at 1, 2, and 4 hours after the AICAR injection from the preinjection period (Fig. 1A; +32%, +59%, and +36%, respectively, from pre; $P < .05$). In the EDL muscle, the phosphorylated AMPKα protein also increased at 1, 2, and 4 hours after the AICAR injection from the preinjection period (Fig. 1B; +150%, +151%, and +150%, respectively, from pre; $P < .05$). Total AMPKα protein expression did not change in the soleus or EDL muscles (Fig. 1C, D).

The effect of AICAR was further examined on the phosphorylation of ACC, a downstream target of AMPK controlling the entry of fatty acids into mitochondrial matrix in skeletal muscle [21]. Fig. 2 shows the change in the phosphorylated and total ACC protein expression after an AICAR treatment. In the soleus muscle, the phosphorylated ACC protein increased at 1 and 2 hours after the AICAR injection from the preinjection period (Fig. 2A; +178% and +101%, respectively, from pre; $P < .05$). In the EDL muscle, the phosphorylated ACC protein also increased at 1, 2, and 4 hours after the AICAR injection from the preinjection period (Fig. 2B; +178%, +392%, and +173%, respectively, from pre; $P < .05$). Total ACC protein expression did not change in the soleus or EDL muscles (Fig. 2C, D).

3.2. SIRT1 protein expression

Fig. 3 shows the change in the SIRT1 protein expression after an AICAR administration. In the soleus muscle, no changes were observed after the treatment (Fig. 3A). In the EDL muscle, the SIRT1 protein increased (+24%) at 24 hours after the treatment from the pretreatment period (Fig. 3B, $P < .05$). In addition, the SIRT1 protein expression in the EDL muscle at 24 hours after the AICAR treatment was significantly higher than that in the saline treatment (Table 1, $P < .05$).

3.3. PGC-1α protein expression

Fig. 4 shows the change of the PGC-1α protein expression after an AICAR administration. The PGC-1α protein increased at 24 hours after an AICAR administration from the pretrial period in both the soleus (Fig. 4A) and EDL (Fig. 4B) muscles (+21% and +26%, respectively, from pre; $P < .05$). In addition, the PGC-1α protein expression in both the soleus and EDL muscles at 24 hours after the AICAR treatment was significantly higher than that in the saline treatment (Table 1, $P < .05$).

3.4. GLUT4 protein expression

Fig. 5 shows the change in the GLUT4 protein expression after an AICAR administration. In the soleus muscle, no changes were observed after the treatment (Fig. 5A). In the

Table 1
Skeletal muscle protein expression and hexokinase activity 24 hours after either saline or AICAR administration

	Soleus muscle		EDL muscle	
	Saline	AICAR	Saline	AICAR
SIRT1 (% of saline)	100.0 ± 1.8	104.1 ± 2.5	100.0 ± 6.2	117.6 ± 2.1*
PGC-1α (% of saline)	100.0 ± 6.0	116.3 ± 3.4*	100.0 ± 6.7	122.0 ± 8.1*
GLUT4 (% of saline)	100.0 ± 4.1	102.5 ± 5.9	100.0 ± 6.9	137.0 ± 5.8*
Hexokinase activity (μmol L^{-1} g^{-1} min^{-1})	2.02 ± 0.07	2.33 ± 0.07*	2.49 ± 0.07	3.45 ± 0.11*

Data are expressed as the mean ± SE; n = 12 muscles per group.
* $P < .05$ vs saline-treated group.

EDL muscle, the GLUT4 protein increased (+38%) at 24 hours after the treatment from the pretreatment period (Fig. 5B, $P < .05$). In addition, the GLUT4 protein expression in the EDL muscle at 24 hours after the AICAR treatment was significantly higher than that in the saline treatment (Table 1, $P < .05$).

3.5. Hexokinase activity

Fig. 6 shows the change in the hexokinase activity after an AICAR administration. In the soleus muscle, the hexokinase activity increased at 18 and 24 hours after an AICAR administration from the pretrial period (Fig. 6A; +12% and +12%, respectively, from pre; $P < .05$). In the EDL muscle, the activity increased at 12, 18, and 24 hours after an AICAR administration from the pretrial period (Fig. 6B; +24%, +36%, and +30%, respectively, from pre; $P < .05$). In addition, the hexokinase activity in both the soleus and EDL muscles at 24 hours after the AICAR treatment was significantly higher than that in the saline treatment (Table 1, $P < .05$).

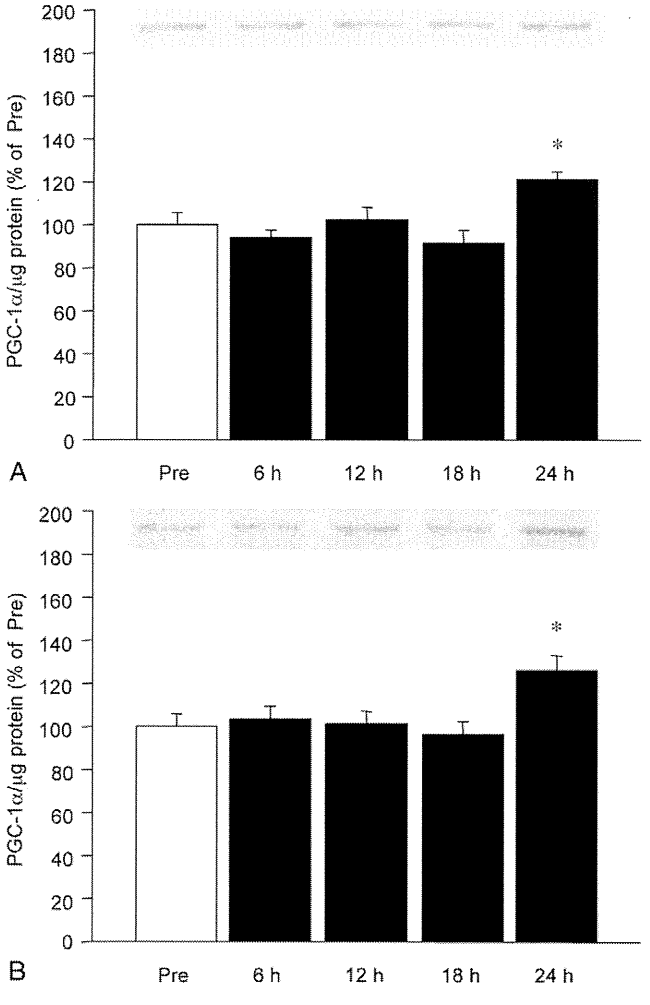

Fig. 4. PGC-1α protein expression in the soleus (A) and EDL (B) muscles before and 6, 12, 18, and 24 hours after AICAR treatment. Values are the means ± SE; n = 12 muscles per group. *$P < .05$ vs pre.

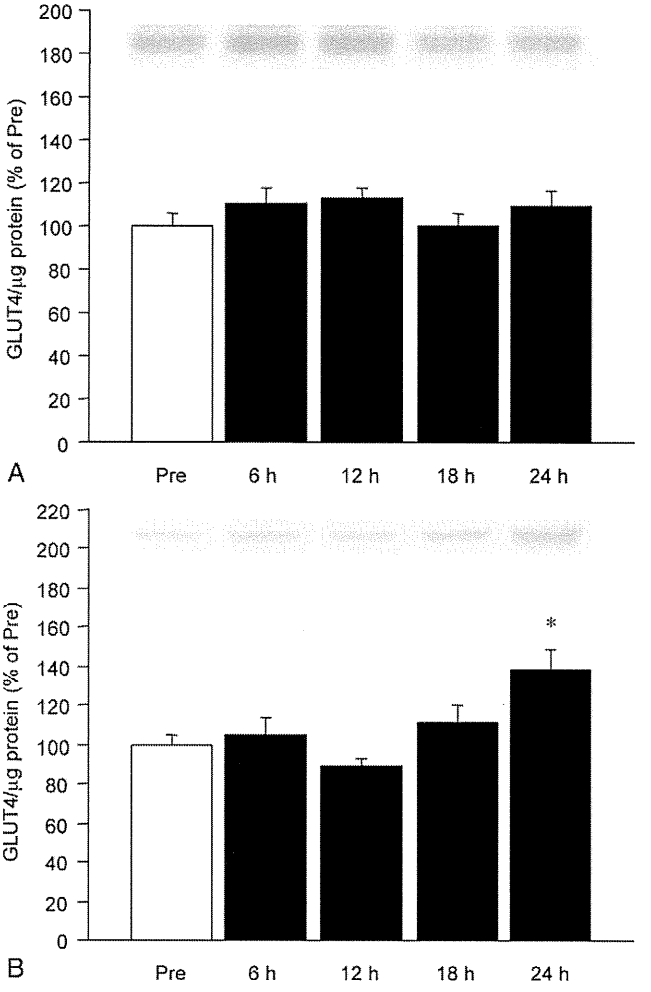

Fig. 5. GLUT4 protein expression in the soleus (A) and EDL (B) muscles before and 6, 12, 18, and 24 hours after AICAR treatment. Values are the means ± SE; n = 12 muscles per group. *$P < .05$ vs pre.

4. Discussion

The current study demonstrated that the activation of AMPK with AMPK activator AICAR treatment in vivo increases the SIRT1 protein expression in the rat EDL muscle. The AMPK phosphorylation level in human hepatoma cell line HepG2 is associated with the SIRT1 protein level [32]. Incubation of HepG2 cells in a high-glucose medium (25 mmol/L) decreases the phosphorylation of AMPK and its downstream target ACC with parallel decline of SIRT1 protein level in comparison to that in low-glucose medium (5 mmol/L). In contrast, incubation of HepG2 cells with pyruvate (0.1 or 1 mmol/L) increases the phosphorylation of AMPK and ACC and SIRT1 protein content. These results suggest that AMPK controls SIRT1 protein content.

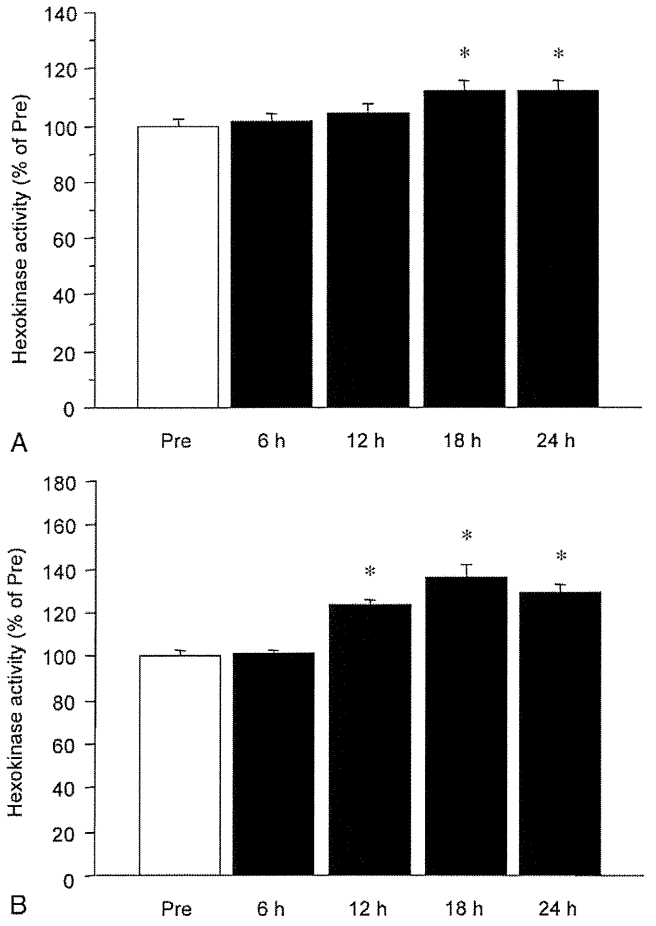

Fig. 6. Hexokinase activity in the soleus (A) and EDL (B) muscles before and 6, 12, 18, and 24 hours after AICAR treatment. Values are the means ± SE; n = 12 muscles per group. *$P < .05$ vs pre.

The effects of AICAR treatment to animals seem similar to those of endurance exercise training with regard to glucose uptake, mitochondrial fatty acid oxidation, and mitochondrial and GLUT4 biogenesis in skeletal muscle [10]. The endurance exercise increased the skeletal muscle SIRT1 protein expression [29]. Consequently, the results regarding SIRT1 in the current study further suggest that the AICAR treatment mimics the benefits of endurance exercise. In skeletal muscle cells, SIRT1 plays an important role in metabolic adaptations including mitochondrial biogenesis, fatty acid oxidation, and glucose homeostasis through deacetylation of PGC-1α [7-9]. Collectively, these observations raise the possibility that the AMPK-SIRT1-PGC-1α pathway may, in part, contribute to the metabolic adaptations with endurance exercise training in skeletal muscle.

However, AMPK may not be the only way to regulate the SIRT1 expression with exercise. The ablation of the AMPK activity experiments using AMPK dominant negative or AMPKα2 knockout mice models demonstrates that AMPK is not always essential for the regulation of downstream targets including ACC, fatty acid oxidation, mitochondrial biogenesis, or the glucose metabolism [33-35], thus suggesting that the redundant signaling pathways cooperate with AMPK in many kinds of adaptations and that signaling other than AMPK may compensate for such metabolic characteristics in the AMPK ablation state. To elucidate the mechanisms, other than AMPK, which regulate the SIRT1 expression with exercise, further experiments using AMPK ablation animal models subjected to various types of exercise are thus called for.

The mechanisms underlying the increase of SIRT1 protein content with AICAR treatment are unclear at present. One potential mechanism for this phenomenon is that nitric oxide synthase (NOS) mediates the SIRT1 expression after an AICAR treatment. The AMPK-induced skeletal and cardiac muscle glucose uptake depends on NOS [36]. In addition, AMPK seems to enhance the NOS activity and phosphorylation of endothelial NOS at Ser^{1177} [36,37]. The level of expression and phosphorylation of endothelial NOS is associated with SIRT1 expression in endothelial cells [38,39]. Furthermore, long-term treatment of NOS inhibitor N^G-nitro-L-arginine-methyl ester decreases the skeletal muscle SIRT1 protein content (M Suwa and S Kumagai, unpublished observation). Overall, it is likely that increasing SIRT1 protein expression with AICAR treatment is mediated by NOS. However, other studies have demonstrated that NOS inhibition does not affect the AICAR- or contraction-induced glucose uptake in rat skeletal muscle [40,41]. Further studies are necessary to clarify the mechanisms in the increase of skeletal muscle SIRT1 dependent on NOS after AMPK activation.

In the current study, the SIRT1 protein expression in the EDL muscle increased with AICAR treatment but not in the soleus. In addition, other characteristics examined in this study indicate inconsistent results between EDL and soleus muscles. The GLUT4 protein expression significantly increased with AICAR in the EDL muscle but not in the soleus muscle. In the hexokinase activity, AICAR treatment also seems more effective to the EDL than soleus muscle. The increase of AMPK phosphorylation level with AICAR in the EDL (~+150% from pre) seems greater than that in soleus (+32%-59% from pre) as well as ACC phosphorylation level (EDL, +173%-391%; soleus, +89%-179%; from pre), raising the possibility that such difference in the effect of AICAR against the AMPK phosphorylation partially causes the different results between soleus and EDL muscles. Another potential cause for such differences in regard to AICAR treatment is the difference in the AMPK subunit isoform distribution between muscle fiber types. The soleus muscle possesses dominantly slow-twitch type I fibers (type I, 84%; type IIA, 7%; type IIX, 9%; type IIB, 0%), whereas EDL muscle possesses dominantly fast-twitch type II fibers (type I, 4%; type IIA, 20%; type IIX, 38%; type IIB, 38%) in rats [42]. In rodents, the γ3-subunit of AMPK is dominantly expressed in the fast-twitch muscle in comparison to the slow-twitch muscle [43]. The γ3-containing AMPK complexes contain only α2- and β2-subunits [43], thus suggesting that α2/β2/γ3 heterotrimer preferentially expressed in the

fast-twitch muscle. Because α2- and β3-subunits play an important role for metabolic and contractile properties in skeletal muscle [44-46], it is likely that the different effects between soleus and EDL muscles on AMPK activation observed in this study are, at least in part, attributable to such differences in the subunit expression pattern between muscle fiber types.

The current study demonstrated that short-term AICAR treatment to rats promotes the skeletal muscle SIRT1 protein expression. On the other hand, a previous study has shown that long-term AICAR treatment to rats for 5 successive days decreases (white gastrocnemius and red and white tibialis anterior muscles) or fails to change (heart and red gastrocnemius muscles) the SIRT1 protein expression [47]. In addition, AICAR treatment for 14 successive days does not alter the SIRT1 protein expression in the rat red and white gastrocnemius muscles (M Suwa and S Kumagai, unpublished observation). These observations suggest that the effect of AICAR treatment on SIRT1 protein expression may thus differ depending on the treatment period. The SIRT1 transcription is regulated by the transcriptional factors E2F transcriptional factor 1 and hypermethylated in cancer 1 [48]. SIRT1 binds to these transcriptional factors, and the complexes repress its transcription [49,50]. This negative feedback loop in SIRT1 regulation might be at least partially associated with the inconsistent results observed among the different treatment period.

Although several previous studies have demonstrated that long-term AICAR treatment enhances the PGC-1α and GLUT4 protein expression and hexokinase activity in the skeletal muscles of rodents in vivo [23,24], the present study is the first to demonstrate that short-term administration of AICAR to rats also promotes them. These results suggest that only a single AICAR treatment is sufficient to promote such phenotypes. Previous studies have demonstrated that short-term endurance exercise augments the PGC-1α and GLUT4 expression and the hexokinase activity and expression [51-53]. These short-term exercise–induced changes may be at least partially associated with AMPK.

Several observations may explain the mechanisms in such changes with AICAR treatment. The PGC-1α and hexokinase II genes have a cyclic AMP–response element, and their transcription is thought to be controlled by the transcriptional factor cyclic AMP–response element binding protein [54-56]. The GLUT4 transcription is regulated by the transcriptional factors myocyte enhancer factor 2 and GLUT4 enhancer factor [57,58]. All these transcriptional factors are phosphorylated and/or transcriptionally activated by AMPK [55,59]. Presumably, such mechanisms are the possible causes for the increase in PGC-1α and GLUT4 expression and hexokinase activity with short-term AICAR treatment.

SIRT1 is associated with insulin sensitivity [7], insulin [60] and adiponectin [61] secretion, mitochondrial biogenesis, fatty acid oxidation [9], protection of neurodegenerative disorders, [62], and longevity [7]. The current study contributes to the understanding of the role of AMPK in the regulation of SIRT1 protein expression and further supports the strategies aimed to activate AMPK as a means of improving the outcome of chronic diseases.

In summary, these results show that short-term AMPK activator AICAR treatment to rats enhances the skeletal muscle AMPK and ACC phosphorylation and then coincidently increases the SIRT1 protein expression. The PGC-1α and GLUT4 protein expression and hexokinase activity also increases with AICAR treatment. Some of these changes preferentially occur in fast-twitch EDL muscles. Therefore, the observations in this study may provide new insights into the mechanisms of SIRT1 regulation and thereby help in both the prevention of and therapy for some chronic diseases including insulin resistance, type 2 diabetes mellitus, metabolic syndrome, and neurodegenerative disorders.

Acknowledgment

This work was supported by a Grant-in-Aid for Scientific Research from the Ministry of Education, Culture, Sports, Science, and Technology of Japan (20700524) to MS.

References

[1] Tissenbaum HA, Guarente L. Increased dosage of a sir-2 gene extends lifespan in *Caenorhabditis elegans*. Nature 2001;410:227-30.
[2] Kaeberlein M, McVey M, Guarente L. The SIR2/3/4 complex and SIR2 alone promote longevity in *Saccharomyces cerevisiae* by two different mechanisms. Genes Dev 1999;13:2570-80.
[3] Blander G, Guarente L. The Sir2 family of protein deacetylases. Annu Rev Biochem 2004;73:417-35.
[4] Fulco M, Sartorelli V. Comparing and contrasting the roles of AMPK and SIRT1 in metabolic tissues. Cell Cycle 2008;7:3669-79.
[5] Sun C, Zhang F, Ge X, et al. SIRT1 improves insulin sensitivity under insulin-resistant conditions by repressing PTP1B. Cell Metab 2007;6: 307-19.
[6] Baur JA, Pearson KJ, Price NL, et al. Resveratrol improves health and survival of mice on a high-calorie diet. Nature 2006;444:337-42.
[7] Lagouge M, Argmann C, Gerhart-Hines Z, et al. Resveratrol improves mitochondrial function and protects against metabolic disease by activating SIRT1 and PGC-1 α. Cell 2006;127:1109-22.
[8] Rodgers JT, Lerin C, Haas W, et al. Nutrient control of glucose homeostasis through a complex of PGC-1α and SIRT1. Nature 2005; 434:113-8.
[9] Gerhart-Hines Z, Rodgers JT, Bare O, et al. Metabolic control of muscle mitochondrial function and fatty acid oxidation through SIRT1/ PGC-1 α. EMBO J 2007;26:1913-23.
[10] Winder WW. Energy-sensing and signaling by AMP-activated protein kinase in skeletal muscle. J Appl Physiol 2002;91:1017-28.
[11] Woods A, Cheung PC, Smith FC, et al. Characterization of AMP-activated protein kinase β and γ subunits. Assembly of the heterotrimeric complex in vitro. J Biol Chem 1996;26:10282-90.
[12] Polekhina G, Gupta A, Michell BJ, et al. AMPK β subunit targets metabolic stress sensing to glycogen. Curr Biol 2003;13:867-71.
[13] Adams J, Chen ZP, Van Denderen BJ, et al. Intrasteric control of AMPK via the gamma1 subunit AMP allosteric regulatory site. Protein Sci 2004;13:155-65.
[14] Stein SC, Woods A, Jones NA, et al. The regulation of AMP-activated protein kinase by phosphorylation. Biochem J 2000;345:437-43.

[15] Sakamoto K, McCarthy A, Smith D, et al. Deficiency of LKB1 in skeletal muscle prevents AMPK activation and glucose uptake during contraction. EMBO J 2005;24:1810-20.
[16] Fujii N, Hayashi T, Hirshman MF, et al. Exercise induces isoform-specific increase in 5′AMP-activated protein kinase activity in human skeletal muscle. Biochem Biophys Res Commun 2000;273:1150-5.
[17] Minokoshi Y, Kim YB, Peroni OD, et al. Leptin stimulates fatty-acid oxidation by activating AMP-activated protein kinase. Nature 2002; 415:339-43.
[18] Yamauchi T, Kamon J, Minokoshi Y, et al. Adiponectin stimulates glucose utilization and fatty-acid oxidation by activating AMP-activated protein kinase. Nat Med 2002;8:1288-95.
[19] Zhou G, Myers R, Li Y, et al. Role of AMP-activated protein kinase in mechanism of metformin action. J Clin Invest 2001;108:1167-74.
[20] Suwa M, Egashira T, Nakano H, et al. Metformin increases the PGC-1α protein and oxidative enzyme activities possibly via AMPK phosphorylation in skeletal muscle in vivo. J Appl Physiol 2006;101: 1685-92.
[21] Merrill GF, Kurth EJ, Hardie DG, et al. AICA riboside increases AMP-activated protein kinase, fatty acid oxidation, and glucose uptake in rat muscle. Am J Physiol Endocrinol Metab 1997;273:E1107-12.
[22] Jessen N, Pold R, Buhl ES, et al. Effects of AICAR and exercise on insulin-stimulated glucose uptake, signaling, and GLUT-4 content in rat muscles. J Appl Physiol 2003;94:1373-9.
[23] Suwa M, Nakano H, Kumagai S. Effects of chronic AICAR treatment on fiber composition, enzyme activity, UCP3, and PGC-1 in rat muscles. J Appl Physiol 2003;95:960-8.
[24] Winder WW, Holmes BF, Rubink DS, et al. Activation of AMP-activated protein kinase increases mitochondrial enzymes in skeletal muscle. J Appl Physiol 2000;88:2219-26.
[25] Leone TC, Lehman JJ, Finck BN, et al. PGC-1α deficiency causes multi-system energy metabolic derangements: muscle dysfunction, abnormal weight control and hepatic steatosis. PLoS Biol 2005;3: e101.
[26] Lin J, Wu H, Tarr PT, et al. Transcriptional co-activator PGC-1α drives the formation of slow-twitch muscle fibres. Nature 2002;418:797-801.
[27] Lan F, Cacicedo JM, Ruderman N, et al. SIRT1 modulation of the acetylation status, cytosolic localization, and activity of LKB1. Possible role in AMP-activated protein kinase activation. J Biol Chem 2008;283:27628-35.
[28] Fulco M, Cen Y, Zhao P, et al. Glucose restriction inhibits skeletal myoblast differentiation by activating SIRT1 through AMPK-mediated regulation of Nampt. Dev Cell 2008;14:661-73.
[29] Suwa M, Nakano H, Radak Z, et al. Endurance exercise increases the SIRT1 and peroxisome proliferator-activated receptor γ coactivator-1α protein expressions in rat skeletal muscle. Metabolism 2008;57: 986-98.
[30] Ferrara N, Rinaldi B, Corbi G, et al. Exercise training promotes SIRT1 activity in aged rats. Rejuvenation Res 2008;11:139-50.
[31] Booth FW, Baldwin KM. Muscle plasticity: energy demand and supply processes. In: Rowell L, Sheperd J, editors. Handbook of physiology. Exercise: regulation and integration of multiple systems. Bethesda, MD: Am Physiol Soc; 1996. p. 1075-123.
[32] Suchankova G, Nelson LE, Gerhart-Hines Z, et al. Concurrent regulation of AMP-activated protein kinase and SIRT1 in mammalian cells. Biochem Biophys Res Commun 2009;378:836-41.
[33] Jørgensen SB, Treebak JT, Viollet B, et al. Role of AMPKα2 in basal, training-, and AICAR-induced GLUT4, hexokinase II, and mitochondrial protein expression in mouse muscle. Am J Physiol Endocrinol Metab 2007;292:E331-E339.
[34] Dzamko N, Schertzer JD, Ryall JG, et al. AMPK-independent pathways regulate skeletal muscle fatty acid oxidation. J Physiol 2008;586:5819-31.
[35] Miura S, Kai Y, Kamei Y, Bruce CR, Kubota N, Febbraio MA, et al. α_2-AMPK activity is not essential for an increase in fatty acid oxidation during low-intensity exercise. Am J Physiol Endocrinol Metab 2009; 296:E47-E55.
[36] Fryer LG, Hajduch E, Rencurel F, et al. Activation of glucose transport by AMP-activated protein kinase via stimulation of nitric oxide synthase. Diabetes 2000;49:1978-85.
[37] Davis BJ, Xie Z, Viollet B, et al. Activation of the AMP-activated kinase by antidiabetes drug metformin stimulates nitric oxide synthesis in vivo by promoting the association of heat shock protein 90 and endothelial nitric oxide synthase. Diabetes 2006;55:496-505.
[38] Ota H, Eto M, Kano MR, et al. Cilostazol inhibits oxidative stress–induced premature senescence via upregulation of Sirt1 in human endothelial cells. Arterioscler Thromb Vasc Biol 2008;28:1634-9.
[39] Nisoli E, Tonello C, Cardile A, et al. Calorie restriction promotes mitochondrial biogenesis by inducing the expression of eNOS. Science 2005;310:314-7.
[40] Higaki Y, Hirshman MF, Fujii N, et al. Nitric oxide increases glucose uptake through a mechanism that is distinct from the insulin and contraction pathways in rat skeletal muscle. Diabetes 2001;50:241-7.
[41] Stephens TJ, Canny BJ, Snow RJ, et al. 5′-Aminoimidazole-4-carboxyamide-ribonucleoside–activated glucose transport is not prevented by nitric oxide synthase inhibition in rat isolated skeletal muscle. Clin Exp Pharmacol Physiol 2004;31:419-23.
[42] Delp MD, Duan C. Composition and size of type I, IIA, IID/X, and IIB fibers and citrate synthase activity of rat muscle. J Appl Physiol 1996; 80:261-70.
[43] Mahlapuu M, Johansson C, Lindgren K, et al. Expression profiling of the γ-subunit isoforms of AMP-activated protein kinase suggests a major role for γ3 in white skeletal muscle. Am J Physiol Endocrinol Metab 2004;286:E194-E200.
[44] Röckl KS, Hirshman MF, Brandauer J, et al. Skeletal muscle adaptation to exercise training: AMP-activated protein kinase mediates muscle fiber type shift. Diabetes 2007;56:2062-9.
[45] Mu J, Brozinick Jr JT, Valladares O, et al. A role for AMP-activated protein kinase in contraction- and hypoxia-regulated glucose transport in skeletal muscle. Mol Cell 2001;7:1085-94.
[46] Garcia-Roves PM, Osler ME, Holmström MH, et al. Gain-of-function R225Q mutation in AMP-activated protein kinase γ3 subunit increases mitochondrial biogenesis in glycolytic skeletal muscle. J Biol Chem 2008;283:35724-34.
[47] Gurd B, Yoshida Y, Lally J, et al. SIRT1 is not associated with oxidative capacity in rat heart and skeletal muscle and its over-expression reduces mitochondrial biogenesis. J Physiol 2009;587: 1817-28.
[48] Zschoernig B, Mahlknecht U. SIRTUIN 1: regulating the regulator. Biochem Biophys Res Commun 2008;376:251-5.
[49] Chen WY, Wang DH, Yen RC, et al. Tumor suppressor HIC1 directly regulates SIRT1 to modulate p53-dependent DNA-damage responses. Cell 2005;123:437-48.
[50] Wang C, Chen L, Hou X, et al. Interactions between E2F1 and SirT1 regulate apoptotic response to DNA damage. Nat Cell Biol 2006;8: 1025-31.
[51] Kraniou GN, Cameron-Smith D, Hargreaves M. Acute exercise and GLUT4 expression in human skeletal muscle: influence of exercise intensity. J Appl Physiol 2006;101:934-7.
[52] O'Doherty RM, Bracy DP, Osawa H, et al. Rat skeletal muscle hexokinase II mRNA and activity are increased by a single bout of acute exercise. Am J Physiol Endocrinol Metab 1994;266:E171-E178.
[53] Mathai AS, Bonen A, Benton CR, et al. Rapid exercise-induced changes in PGC-1α mRNA and protein in human skeletal muscle. J Appl Physiol 2008;105:1098-105.
[54] Osawa H, Robey RB, Printz RL, et al. Identification and characterization of basal and cyclic AMP response elements in the promoter of the rat hexokinase II gene. J Biol Chem 1996;271:17296-303.
[55] Thomson DM, Herway ST, Fillmore N, et al. AMP-activated protein kinase phosphorylates transcription factors of the CREB family. J Appl Physiol 2008;104:429-38.
[56] Herzig S, Long F, Jhala US, et al. CREB regulates hepatic gluconeogenesis through the coactivator PGC-1. Nature 2001;413: 179-83.

[57] Oshel KM, Knight JB, Cao KT, et al. Identification of a 30-base pair regulatory element and novel DNA binding protein that regulates the human GLUT4 promoter in transgenic mice. J Biol Chem 2000;275: 23666-73.

[58] Thai MV, Guruswamy S, Cao KT, et al. Myocyte enhancer factor 2 (MEF2)–binding site is required for GLUT4 gene expression in transgenic mice. Regulation of MEF2 DNA binding activity in insulin-deficient diabetes. J Biol Chem 1998;273:14285-92.

[59] Holmes BF, Sparling DP, Olson AL, et al. Regulation of muscle GLUT4 enhancer factor and myocyte enhancer factor 2 by AMP-activated protein kinase. Am J Physiol Endocrinol Metab 2005;289: E1071-6.

[60] Bordone L, Motta MC, Picard F, et al. Sirt1 regulates insulin secretion by repressing UCP2 in pancreatic β cells. PLoS Biol 2006;4:e31.

[61] Qiang L, Wang H, Farmer SR. Adiponectin secretion is regulated by SIRT1 and the endoplasmic reticulum oxidoreductase Ero1-L α. Mol Cell Biol 2007;27:4698-707.

[62] Kim D, Nguyen MD, Dobbin MM, et al. SIRT1 deacetylase protects against neurodegeneration in models for Alzheimer's disease and amyotrophic lateral sclerosis. EMBO J 2007;26:3169-79.

Free Radical Biology & Medicine 51 (2011) 417–423

Contents lists available at ScienceDirect

Free Radical Biology & Medicine

journal homepage: www.elsevier.com/locate/freeradbiomed

Original Contribution

Age-dependent changes in 8-oxoguanine-DNA glycosylase activity are modulated by adaptive responses to physical exercise in human skeletal muscle

Zsolt Radak [a,*], Zoltan Bori [a], Erika Koltai [a], Ioannis G. Fatouros [b], Athanasios Z. Jamurtas [c], Ioannis I. Douroudos [b], Gerasimos Terzis [d], Michalis G. Nikolaidis [e], Athanasios Chatzinikolaou [b], Apostolos Sovatzidis [f], Shuzo Kumagai [a,g], Hisahi Naito [h], Istvan Boldogh [i]

[a] Research Institute of Sport Science, Semmelweis University, Budapest H-1123, Hungary
[b] Department of Physical Education and Sport Science, Democritus University of Thrace, Komotini 69100, Greece
[c] Department of Physical Education and Sport Science, University of Thessaly, Trikala 42100, Greece
[d] Laboratory of Athletics, School of Physical Education and Sport Science, University of Athens, Daphne 17237, Athens, Greece
[e] Institute of Human Performance and Rehabilitation, Centre for Research and Technology–Thessaly, Trikala, Greece
[f] Medical School, Democritus University of Thrace, Alexandroupolis, Greece
[g] Kyushu University, Fukuoka, Japan
[h] Department of Exercise Physiology, School of Health and Sport Science, Juntendo University, Chiba, Japan
[i] Department of Microbiology and Immunology, University of Texas Medical Branch at Galveston, Galveston, TX 77555, USA

ARTICLE INFO

Article history:
Received 13 January 2011
Revised 6 April 2011
Accepted 11 April 2011
Available online 15 April 2011

Keywords:
Exercise
Aging
DNA damage/repair
Sirtuins
Antioxidants
8-OxoG
OGG1
Acetylation
Free radicals

ABSTRACT

8-Oxo-7,8-dihydroguanine (8-oxoG) accumulates in the genome over time and is believed to contribute to the development of aging characteristics of skeletal muscle and various aging-related diseases. Here, we show a significantly increased level of intrahelical 8-oxoG and 8-oxoguanine-DNA glycosylase (OGG1) expression in aged human skeletal muscle compared to that of young individuals. In response to exercise, the 8-oxoG level was lastingly elevated in sedentary young and old subjects, but returned rapidly to preexercise levels in the DNA of physically active individuals independent of age. 8-OxoG levels in DNA were inversely correlated with the abundance of acetylated OGG1 (Ac-OGG1), but not with total OGG1, apurinic/apyrimidinic endonuclease 1 (APE1), or Ac-APE1. The actual Ac-OGG1 level was linked to exercise-induced oxidative stress, as shown by changes in lipid peroxide levels and expression of Cu,Zn-SOD, Mn-SOD, and SIRT3, as well as the balance between acetyltransferase p300/CBP and deacetylase SIRT1, but not SIRT6 expression. Together these data suggest that that acetylated form of OGG1, and not OGG1 itself, correlates inversely with the 8-oxoG level in the DNA of human skeletal muscle, and the Ac-OGG1 level is dependent on adaptive cellular responses to physical activity, but is age independent.

Age-associated increases in levels of reactive oxygen species (ROS), especially during the last quarter of life, result in excessive oxidative damage to macromolecules, including DNA [1–5]. Among DNA and RNA bases, guanine is predominantly prone to oxidation because of its lowest reduction potential [6]. It is modified primarily by hydroxyl radicals at or near diffusion-controlled rates (reviewed in [7–9]). More than 20 oxidation products of the guanine base have been identified [10] and among them one of the most abundant is 8-oxo-7,8-dihydroguanine (8-oxoG) [7–9]. In DNA, the 8-oxoG level increases upon radiation, ischemia/reperfusion, acute exercise, and aging [4,11–14]. 8-OxoG is excised from DNA by formamidopyrimidine-DNA glycosylase (Fpg) in *Escherichia coli* and by its functional homolog 8-oxoguanine-DNA glycosylase (OGG1) in mammals in the base excision repair (BER) pathway [15–18]. Whereas Fpg is well known to excise 4,6-diamino-5-formamidopyrimidine (FapyA), 2,6-diamino-4-hydroxy-5-formamidopyrimidine (FapyG), and 8-oxoG with nearly similar excision kinetics [18,19], the mammalian and yeast OGG1 is specific for 8-oxoG and FapyG, but not FapyA [20,21]. When 8-oxoG is not repaired, it is mutagenic, as it has been shown to pair with adenine (A) instead of cytosine (C) and thereby induces G:C→T:A transversions [15,22].

It is documented that in covalent modifications of DNA repair proteins, e.g., by acetylation, phosphorylation plays a significant role, particularly in their repair activity, which consists of the removal/repair of oxidative base lesions [23,24]. In fact, it has been shown that OGG1 and human apurinic/apyrimidinic endonuclease 1 (APE1) activities are primarily regulated by p300/CBP-mediated acetylation reactions, processes that significantly influence their repair activities and hence cell fate [23–25]. The role of sirtuin family deacetylases has gathered considerable attention [26], as SIRT1 and SIRT6 have been shown to be

* Corresponding author. Fax: +36 1 356 6337.
E-mail address: radak@mail.hupe.hu (Z. Radak).

0891-5849/$ – see front matter © 2011 Elsevier Inc. All rights reserved.
doi:10.1016/j.freeradbiomed.2011.04.018

involved in DNA repair [27–29]. An increased deacetylase activity of sirtuins may lead to a decrease in acetylation levels of proteins, which, in turn, would result in a decline in enzymatic activities, including those of OGG1 and APE1.

Although it is well documented that acetylation increases OGG1 activity in cell cultures and in vitro assays, the existence of acetylated OGG1 (Ac-OGG1) and APE1 (Ac-APE1) under in vivo conditions is still unknown. The goals of this investigation were (a) to determine changes in Ac-OGG1 and Ac-APE1 in human skeletal muscle, (b) to study the effects of aging and acute as well as regular physical conditioning on acetylation levels of these DNA repair enzymes, and (c) to evaluate the possible roles of SIRT1, SIRT3, and SIRT6 in the adaptability of human skeletal muscle. This report shows that the level of acetylated OGG1 changes as a function of age, and exercise training increases this posttranslational modification independent of age in human muscles.

Materials and methods

Subjects

Forty-eight healthy men volunteered to participate in this study. A written informed consent was signed by all participants regarding their participation after they were told of all risks, discomforts, and benefits involved in the study. Procedures were in accordance with the Helsinki Declaration of 1975 and were approved by the ethics committee of the University of Thessaly.

Participants were assigned to one of four groups according to a cross-over, repeated-measures design: (a) young sedentary (YS; 26.0 ± 4.5 years), (b) young physically active (YA; 30.2 ± 7.9 years), (c) old sedentary (OS; 63.4 ± 4.7 years), and (d) old physically active (OA; 62.4 ± 2.9 years). Subjects were exposed to a single bout of the exercise protocol and muscle biopsies were taken. Participants were assigned to the young or old sedentary group based on a maximal oxygen uptake (VO_{2max}) of below 25 ml/kg/min for old participants and below 35 ml/kg/min for young participants, and the young and old physically active groups were based upon the ACSM description [30], VO_{2max} over 45 ml/kg/min for young participants and over 35 ml/kg/min for old (YS, 35.9 ± 4.7; OS, 25.1 ± 3.0; YA, 51.8 ± 7.9; OA, 37.1 ± 2.9 ml/kg/min).

Participants visited the laboratory on three occasions. During their first visit, participants were examined by a trained physician for limiting health complications; in their second visit, participants had their body height/weight and skin-folds measured and underwent a Graded Exercise Testing (GXT) to evaluate their VO_{2max}. During their third visit, a week later, participants underwent a submaximal exercise bout to exhaustion on the treadmill, and muscle biopsies were collected before and after exercise.

Measurement of peak oxygen uptake (VO_{2peak})

VO_{2peak} was determined during a GXT on a treadmill to voluntary exhaustion as previously described [31].

Exercise protocol

A single bout of exercise included initially 45 min of running on a treadmill at 70–75% of the subject's VO_{2max}. After 45 min, the speed increased to 90% of VO_{2max}, and exercise was terminated at exhaustion [32].

Muscle biopsy sampling

Participants had been instructed to refrain from physical activity and caffeine consumption for 48 h before exercise. Both muscle specimens (pre- and postexercise), of approximately 100–120 mg each, were obtained from the vastus lateralis of the same leg of each participant by using the needle biopsy technique [33]. The first biopsy was obtained approximately 20 cm away from the midpatella of the right (dominant) leg with the application of suction [34].

Assessment of malondialdehyde levels

Blood samples were collected from an antecubital arm vein into evacuated tubes containing ethylenediaminetetraacetic acid. Plasma was separated by centrifugation (1500 *g*, 4 °C, for 15 min). Samples were stored at −80 °C. Malondialdehyde (MDA) levels were measured by reverse-phase, high-performance liquid chromatography (HPLC) with fluorimetric detection (excitation 532 nm and emission 550 nm) as described [35].

Real-time quantitative RT-PCR

Total RNA from skeletal muscle samples (~30 mg) was extracted with NucleoSpin RNA/protein (Macherey-Nagel, Düren, Germany) according to the manufacturer's protocol. Analyses of the real-time quantitative PCR data were performed using the comparative threshold cycle (C_t) method, as suggested by Applied Biosystems (User Bulletin 2). The primers used are listed in Table 1.

Fluorescence imaging and quantification

At optimal cutting, temperature-fixed, paraffin-embedded muscles were sectioned into 5-μm sections. The measurement of 8-oxoG levels in nuclear DNA of muscles was assessed by quantitative microscopic imaging, as we previously described [23,36]. Briefly, sections were deparaffinized, air-dried, and fixed in acetone:methanol (1:1), rehydrated in PBS for 15 min, and then sequentially treated with RNase (100 μg/ml) for 15 min followed by 100 μg/ml pepsin in the presence of 0.1 N HCl for 30 min at 37 °C. The sections were washed and then incubated with affinity-purified, nonimmune IgG (100 μg/ml) for 30 min and washed in PBS containing 0.5% bovine serum albumin and 0.1% Tween 20 (PBS-T). After incubation with anti-8-oxoG antibody (Trevigen, Gaithersburg, MD, USA; 1:300 dilution) [37] for 30 min, the sections were washed for 15 min three times with PBS-T and then binding of primary antibody was detected with conjugated secondary antibody.

Table 1
Primers used in RT-PCR.

	Primer sequence
Reference gene	
β-Actin	Forward: 5′-GCTCGTCGTCGACAACGGCTC-3′
β-Actin	Reverse: 5′-CAAACATGATCTGGGTCATCTTCT-3′
RP28S	Forward: 5′-AGCCGATCCATCATCCGCAATG-3′
RP28S	Reverse: 5′-CAGCCAAGCTCAGCGCAAC-3′
Target gene	
OGG1	Forward: 5′-GTGGACTCCCACTTCCAAGA-3′
OGG1	Reverse: 5′-GAGATGAGCCTCCACCTCTG-3′
EP300	Forward: 5′-TCATCTCCGGCCCTCTCGGC-3′
EP300	Reverse: 5′-GCTCTGTTGGGCCTGGCTGG-3′
SIRT1	Forward: 5′-TGCGGGAATCCAAAGGATAATTCAGTGTC-3′
SIRT1	Reverse: 5′-CTTCATCTTTGTCATACTTCATGGCTCTATG-3′
SIRT3	Forward: 5′-GTCGGGCATCCCTGCCTCAAAGC-3′
SIRT3	Reverse: 5′-GGAACCCTGTCTGCCATCACGTCAG-3′
SIRT6	Forward: 5′-GAGGAGCTGGAGCGGAAGGTGTG-3′
SIRT6	Reverse: 5′-GGCCAGACCTCGCTCCTCCATGG-3′
SOD1	Forward: 5′-AGGGCATCATCAATTTCGAG-3′
SOD1	Reverse: 5′-ACATTGCCCAAGTCTCCAAC-3′
SOD2	Forward: 5′-GCAGAAGCACAGCCTCCCCG-3′
SOD2	Reverse: 5′-CCTTGGCCAACGCCTCCTGG-3′
XRCC6 (Ku70)	Forward: 5′-CTGTCCAAGTTGGTCGCTTC-3′
XRCC6 (Ku70)	Reverse: 5′-CTGCCCCTTAAACTGGTCAA-3′

OGG1 and Ac-OGG1 levels were also determined via quantitative microscopic imaging [36,38]. Purified mouse anti-OGG1 antibody (human OGG1 reactive) generated against a synthetic peptide (C-DLRQSRHAQEPPAK-N) representing the C-terminus of OGG1 was acquired from Antibodies-Online (Atlanta, GA, USA). The immunogen affinity-purified, human-reactive rabbit polyclonal antibody to Ac-OGG1 was generated against an Ac-Lys-containing peptide (PAKRR^{Ac}KG G^{Ac}KGPEC) [23] obtained from AbCam (Cat. No. ab93670) [23,36]. Antibody reactive with human APE1 [39] and rabbit anti-Ac-APE1 antibody were characterized previously [40]. Binding of primary antibodies was visualized with fluorochrome-labeled secondary antibodies. Confocal microscopic evaluations were performed on a Zeiss LSM510 META system using the 488-nm line of the argon laser for excitation of FITC and the helium–neon 543-nm line for excitation of rhodamine, combined with appropriate dichroic mirrors and emission band filters to discriminate between green and red fluorescence. Images were captured at a magnification of 60 (60× oil immersion objective; numerical aperture 1.4). To objectively quantify fluorescence intensities morphometric analyses were done by using MetaMorph software version 9.0r (Universal Imaging Corp., Downingtown, PA, USA) as we have described [38]. Specifically, images were obtained from >15 fields per muscle section containing 160–180 nuclei and reassembled using the montage stage stitching algorithm of the Metamorph software [41]. Colocalization was visualized by superimposition of green and red images using MetaMorph software version 9.0r.

Statistical analyses

Statistical significance was assessed by three-way ANOVA (age × physical activity status × time), followed by Tukey's post hoc test. The significance level was set at $p<0.05$.

Results

Changes in 8-oxoG level in DNA as a function of age and physical activity in human skeletal muscle

DNA glycosylase/apurinic/apyrimidinic (AP) lyase activity of OGG1 declines with age [42–44]. Here, first we investigated the association between abundance of 8-oxoG in DNA and OGG1, as well as Ac-OGG1 in nuclei of skeletal muscle of OS and YS individuals. Results from quantitative fluorescence intensity analysis showed that there was a significant ($p<0.01$) increase in genomic 8-oxoG (8-oxodG; Fig. 1A) and total OGG1 ($p<0.01$) levels in skeletal muscle

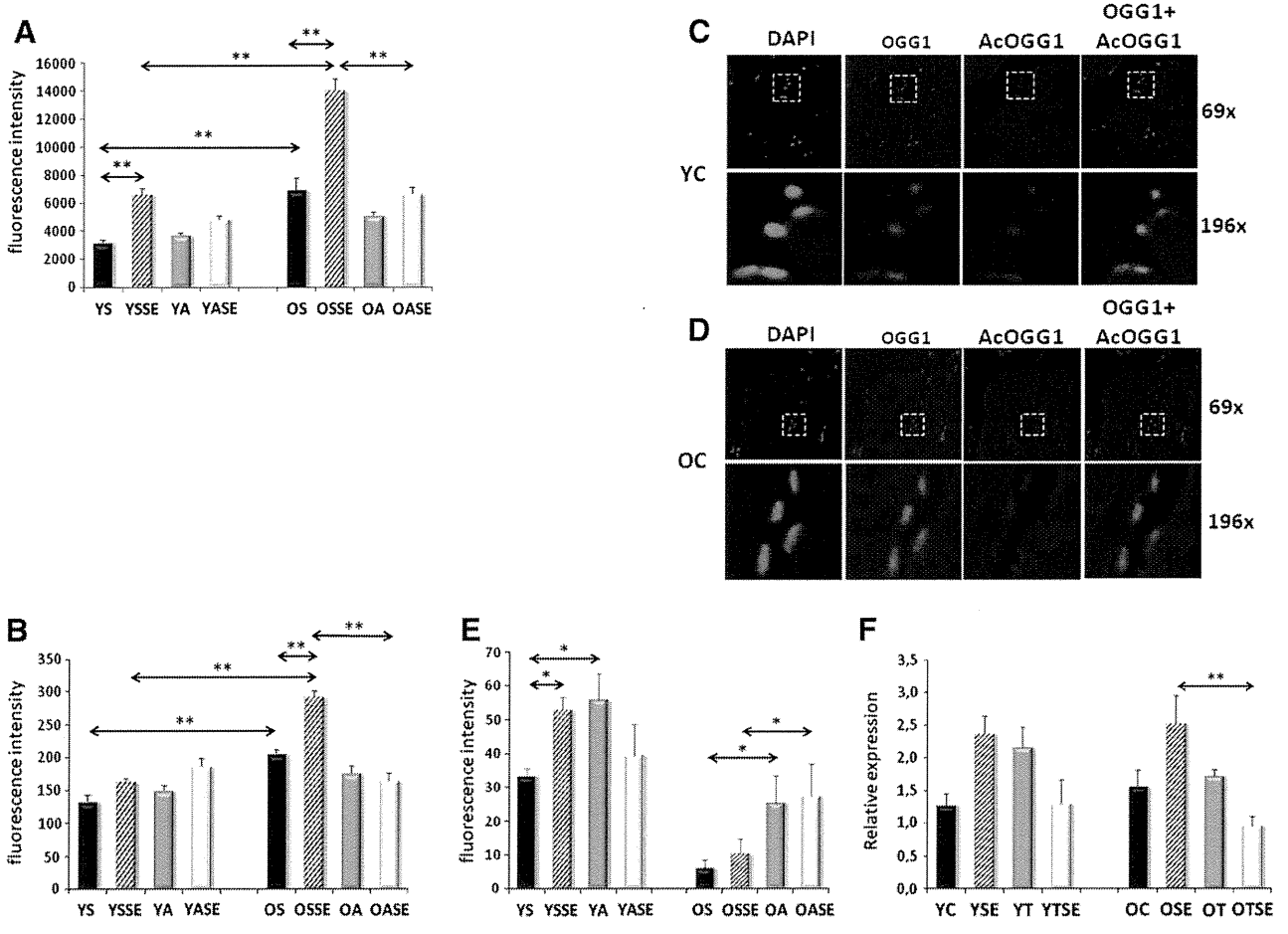

Fig. 1. 8-OxoG, OGG1, and Ac-OGG1 levels in skeletal muscle (SkM) before and after single exercise bout (SEB). (A) Increase in 8-oxoG level in genomic DNA of aged muscles and in response to SEB. (B) Total OGG1 level in SkM of sedentary and physically active subjects. In (A) and (B), sections were stained and fluorescence intensities were analyzed using a montage stage stitching algorithm of the MetaMorph software (Materials and methods). (C) Representative fluorescence images of OGG1 and Ac-OGG1 in sections from the muscles of young individuals. Top: original magnification 69×. Bottom: original magnification 196×. Leftmost images are DAPI, the rightmost images are the superimposition of the OGG1- and Ac-OGG1-mediated fluorescence images. (D) Representative fluorescence images of OGG1 and Ac-OGG1 in muscle sections of old volunteers. Top: original magnification 69×. Bottom: original magnification 196×. Leftmost images are DAPI-stained, the rightmost images are the superimposition of OGG1- and Ac-OGG1-mediated fluorescence images. (E) Changes in Ac-OGG1 levels in skeletal muscle of young and elderly subjects in response to SEB. (F) The relative expression of OGG1 mRNA is shown. DAPI, 4′,6′-diamino-2-phenylindole; YS, young sedentary; YSSE, young sedentary after a single bout of exercise; YA, young active; YASE, young active after a single bout of exercise; OS, old sedentary; OSSE, old sedentary after a single bout of exercise; OA, old active; and OASE, old active after a single bout of exercise. Values are means ± SE for six subjects per group. *$p<0.05$, **$p<0.01$.

of elderly compared to young participants (Fig. 1B). This paradoxical observation suggests an increase in oxidative stress and/or decrease in OGG1 activity; the latter may be due to altered OGG1 posttranslational modification(s), such as acetylation [23]. The acetylated form of OGG1, compared to the unacetylated form, shows an approximately 10-fold increase in repair activity [23]. Immunohistochemical analysis shows that the level of Ac-OGG1 was significantly higher in the skeletal muscle of young individuals (Fig. 1C, top and bottom) compared to that of older subjects. Ac-OGG1 was nearly undetectable in the skeletal muscle of the elderly (Fig. 1D, top and bottom). As calculated from fluorescence intensities, only $5.1 \pm 2.5\%$ of total OGG1 was acetylated in the old, whereas $24.5 \pm 6\%$ of total OGG1 reacted with anti-Ac-OGG1 antibody in the young individuals (Fig. 1E). APE1 is a multifunctional and abundant protein [39] and has been shown to stimulate 8-oxoG repair initiated by OGG1 during BER [45]. Because of APE1's abundance, it was not surprising to observe that its level was not different in the muscle of the young and old groups (data not shown). Ac-APE1 [46] levels were substantially higher only in skeletal muscle of YS individuals compared to that of OS subjects (Fig. 2A); not the APE1 level but the Ac-APE1, together with Ac-OGG1, plays a role in the repair of 8-oxoG. These results support the hypothesis that an increase in the genomic 8-oxoG level is associated with an inability of aged skeletal muscle to posttranslationally modify OGG1 [25].

OGG1's acetylation level is altered by the activity of acetyltransferase p300/CBP [23,25] and deacetylases such as sirtuins [27]. Our results show that expression of p300/CBP is increased ($p<0.01$) in skeletal muscle of OS subjects compared to that in younger counterparts (Fig. 2B). On the other hand, expression of SIRT1 and SIRT6 (Figs. 2C and E) was not affected by age, whereas SIRT3 expression was significantly lower in the OS compared to the YS group (Fig. 2D). In controls, there were no differences in the expression of Ku70 (binds directly to free DNA ends) in the muscles of young and old individuals (Fig. 3A), an indication that the repair efficiency of 8-oxoG is unaffected by age and level of unrepaired AP sites, and DNA single-strand breaks are not sufficient to alter the expression of Ku70.

Oxidative stress induced by physical activity mediates an adaptive response for efficient oxidative DNA damage repair

Old and young physically inactive and active individuals were subjected to a single exercise bout (SEB). SEB-induced changes in oxidative stress levels were determined indirectly by measuring the levels of the lipid peroxidation product MDA in plasma (YS, 0.176 ± 0.02; YSSE, 0.262 ± 0.03*; YA, 0.143 ± 0.01; YASE, 0.181 ± 0.02; OS, 0.254 ± 0.04; OSSE, 0.338 ± 0.06*; OA, 0.188 ± 0.03; OASE, 0.233 ± 0.03 μmol/L; *$p<0.05$). It is obvious that the MDA level was significantly increased only in the plasma of physically inactive old and young subjects. Although we recognize the limitations of MDA measurements [47], the strong match between MDA and 8-oxoG ($p=0.001$) levels suggests that indeed aging and SEB elevate the level of oxidative damage. These results are supported by the observed increase in the expression of Cu,Zn-SOD (Fig. 3B) in the muscle of physically inactive (old and young) subjects. Mn-SOD expression is increased in response to SEB only in young subjects (Fig. 3C). Surprisingly, Mn-SOD expression was not affected by SEB in active/trained old and young individuals (Fig. 3C). Together these data imply an adaptive response of the skeletal muscle to SEB in trained/active individuals.

An increase in MDA level predicts enhanced genomic 8-oxoG levels upon exercise. Thus we asked if regular physical exercise-induced antioxidant responses protect guanine from oxidation in the DNA from muscle biopsies of sedentary vs trained and young vs old subjects. In response to a SEB, the 8-oxoG level was doubled in the muscle of all individuals regardless of whether they were sedentary or physically active. Importantly, whereas 8-oxoG levels returned to

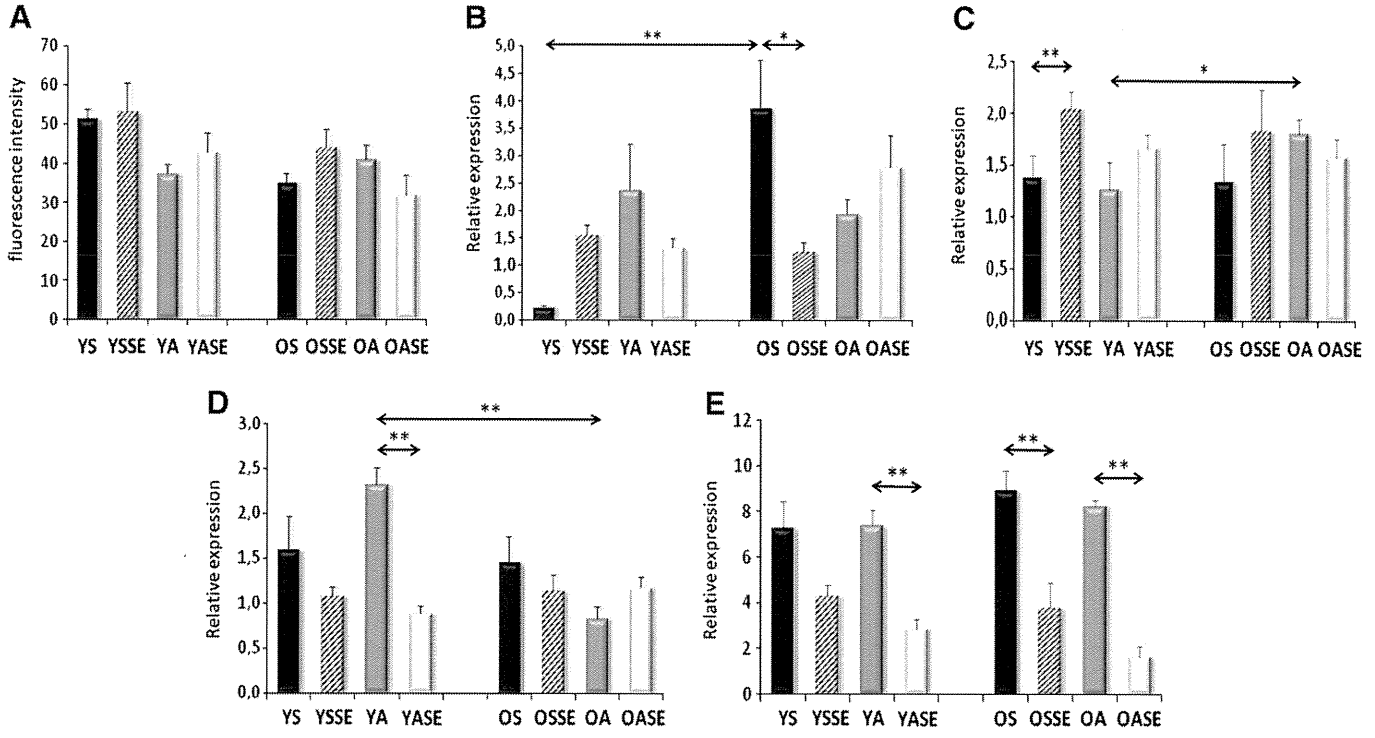

Fig. 2. Ac-APE1 level and expression of p300/CBP, SIRT1, SIRT3, and SIRT6 before and after physical exercise in skeletal muscle. (A) Level of Ac-APE1 as assessed by fluorescence imaging (analyzed as for Fig. 1A). (B–E) Expression at the mRNA level of (B) p300/CBP, (C) SIRT1, (D) SIRT3, and (E) SIRT6. RNA was isolated from muscle biopsies excised before and 24 h after SEB. Quantitative RT-PCR was undertaken as described under Materials and methods. YS, young sedentary; YSSE, young sedentary after a single bout of exercise; YA, young active; YASE, young active after a single bout of exercise; OS, old sedentary; OSSE, old sedentary after a single bout of exercise; OA, old active; and OASE, old active after a single bout of exercise. Values are means ± SE for six subjects per group. *$p<0.05$, **$p<0.01$.